Nonlocal Interaction Induces the Self-organized Mussel Beds*

Guiquan Sun[1,2,†], Shumin Liu[2], Li Li[3,4], Jing Li[5] and Zhen Jin[2]

Abstract Mussel beds are important habitats and food sources for biodiversity in coastal ecosystems. The predation of mussel on algae depends not only on the current time and location, but also on the quantity of algae at other spatial location and time. To know the impacts of such predation behavior on the dynamics of mussel beds well, we pose a reaction-diffusion mussel-algae model coupling nonlocal interaction with kernel function. By calculating the critical conditions of Hopf bifurcation and Turing bifurcation, the conditions for the generation of Turing pattern are obtained. We find that the diffusion rate and predation rate of mussels have effect on the structure and density of spatial pattern of mussels under the nonlocal interaction, and the predation rate of mussels can produce different pattern types, while the diffusion rate plays a more important role on the pattern density. Moreover, the nonlocal interaction promotes the stability of the mussel beds. These results suggest that the nonlocal interaction between mussels and algaes is one of the important mechanisms for the formation of the spatial structure of mussel beds.

Keywords Nonlocal interaction, Mussel-algae system, Hopf bifurcation, Turing pattern, Multi-scale analysis.

MSC(2010) 35B32, 35B36, 37G10, 92B05.

1. Introduction

Mussel beds provide an important habitat of biodiversity and food source of marine ecosystem, and the stability of mussel beds play an important role in marine

ecosystem. Therefore, it is of great significance to mussel beds [20, 22, 23, 27, 45]. Mussels that accumulating in soft sediments usually survive by feeding on algaes which in the lower water layers [38, 42]. Since mussel is largely dependent on the density of the algae for their survival, and the low density of algae maybe leads to the depletion of the mussel beds [8]. In addition, in order to compete for the algae, the mussel usually tend to cluster in the water where the algae gathers [23]. Given that the algae is the main food source of mussel population, many ecologists and mathematicians have thus focused on the interaction between mussel and algae [3, 23, 30, 40].

Experimental studies have shown that mussel gathers to form different spatial distributions due to competition and survival [30], and such phenomenon is called a self-organizing behavior, which is of great significance to the stability existence and restoration of ecological environment [12,18,21,32–34,44]. In fact, mussel population develops self-organizing patterns in two different spatial scales: mussel population forms linear clusters driven by individuals' aggregation behaviors in small spatial scale, which is a rapid process, namely about a day [22,25]; while mussel population produce large, regular zones perpendicular to the flow of water in large spatial scale based on the ecological feedback mechanism (local promotion of algae and large-scale competition of mussel) [30]. The coupling of two forms of self-organization enhances the persistence and robustness of mussel beds compared to non-organized river beds. Therefore, it is necessary to study pattern formation mechanism of mussel beds [30]. Van de Koppel et al. studied the mussel-algae system by using the reaction-diffusion-advection equation [23] for the first time:

$$
\begin{cases}
\dfrac{\partial A}{\partial t} = (A_{up} - A)f - \dfrac{c}{h}AM - V\dfrac{\partial A}{\partial X}, \\[2mm]
\dfrac{\partial M}{\partial t} = ecAM - d_M\dfrac{k_M}{k_M + M}M + D\dfrac{\partial^2 M}{\partial X^2}.
\end{cases}
\tag{1.1}
$$

This paper mainly reported regular spatial pattern of young mussel beds on soft sediments in the Wadden Sea [24]. It has been also proposed that the scale dependent mechanism leads to the spatial self-organization of mussels, which provides a possible explanation for the spatial pattern. Based on this model, Wang et al. analyzed the differential-flow instability conditions that cause the formation of spatial patterns and the influence of parameters on the spatial pattern, and it has also been found that the spatial pattern is the result of the interaction of nonlinear terms [40]. The following literature mainly considered that movement of the algae depends on the flow of water, while ignore the random diffusion of the algae. Thus, a new model with respect to random diffusion of the algae was proposed by Cangelosi et al. [3]:

$$
\begin{cases}
\dfrac{\partial A}{\partial t} = (A_{up} - A)\rho - \dfrac{c}{H}AM - V\dfrac{\partial A}{\partial X} + D_A\triangle A, \\[2mm]
\dfrac{\partial M}{\partial t} = ecAM - d_M\dfrac{k_M}{k_M + M}M + D_M\triangle M,
\end{cases}
\tag{1.2}
$$

the interaction between the young mussel beds and algaes has been studied by using the weak nonlinear diffusion instability analysis method, and the transverse diffusion coefficient of algae which introduced in this system has been obtained by using the spectral analysis method [3].

In fact, many scholars have studied the spatial pattern formed by biological interaction, which has important significance for exploring the possibility of coexis-

tence, persistence and stability among species [14, 19, 35, 36, 39]. Many factors that influencing the type and formation mechanism of the spatial pattern have been studied and considered, such as: time delay, noise, spatiotemporal delay, nonlocal effect and so on [2, 6, 17, 26, 46, 47]. As for the mechanism of mussel's spatial pattern due to self-organizing, there are two possible explanations. The one is scale dependent mechanism, which was proposed by Koppel et al. in 2005. He pointed out that short distance can promote each other between mussels protection from the impact of waves and currents, and long distance is beneficial for high density mussels to compete algae so as to induce the spatial pattern [23]. The other one is sediment accumulation mechanism, which was proposed by Liu et ai. in 2012, indicating that there is a positive feedback effect between sediment accumulation and mussel growth [1, 25, 27, 43]. The prediction of self-organized spatial pattern and study of its formation mechanism have important influence on the improvement of ecosystem productivity and the maintenance of biodiversity [40].

Above all analysis and researches are under the effect of local interaction, in fact, due to the dispersal of the population itself and movement under the action of the wave, the nonlocal effect is very common in the coastal ecosystem. In fact, nonlocal interactions between populations have been introduced and studied not only in coastal systems, but also in many systems [10, 28, 29, 31, 41, 48]. As we know, mussels move in all directions of space to feed on the algae. Therefore, in this paper, we will introduce the nonlocal interaction item in the mussel-algae system to describe the spatial dynamics of mussels so as to describe the interaction between them from the more perspectives. Meanwhile, it provides more possibility explanations for the study of the spatial pattern.

The rest of this paper is introduced as follows: In the second part, a new mussel-algae system with nonlocal interaction is constructed. In the third part, we carry out the dynamics analysis to give the occurrence conditions of Hopf bifurcation and Turing instability. In the fourth part, we use the multi-scale analysis method to obtain the amplitude equation under different conditions of Turing instability. In the last part, numerical simulations are utilized to verify the above theoretical results. Besides, various Turing patterns are shown.

2. Mathematical model

In this section, we introduce the nonlocal interaction term into the mussel-algae system proposed by Van de Koppel et al. [23] and construct a new model. Then, we further analyze the conditions for the system to giving rise to Hopf bifurcation and Turing instability.

It is well-known that the nonlocal reaction-diffusion equation can reflect the interaction between populations more accurately and objectively [4, 13, 15, 37]. Nonlocal interaction is common in coastal ecosystems. The previous analysis and researches considered that algaes are captured by mussels at the same location and time. In fact, it is worth noting that the mussels feed on algae are not only related to the current position and time, but also depend on the density of algae on the whole space at different time, and that is mussels can prey on algae at different time throughout the whole space. As shown in Figure 1, the mussels can not only feed on nearby algaes, but also prey on other algaes in the lower layer through self-diffusion and water flow. Now, we describe the phenomenon by the following

nonlocal interaction term:

$$\int_{-\infty}^{t}\int_{R^2}K(x-y,t-s)A(y,s)dsdy,$$

and the kernel function is

$$K(x,t)=\frac{1}{4\pi t}e^{-\frac{|x|^2}{4t}}\frac{1}{\tau}e^{-\frac{t}{\tau}},$$

we use the above kernel function to describe the spatial nonlocal interaction of the mussel at the time of $t-s$ and the position of $x-y$ capturing the algae at the time of s and the position of y.

Algae with an average density of A_{up} in the upper layer.

Algae with an average density of A in the lower layer.

Soft Sediment Layer
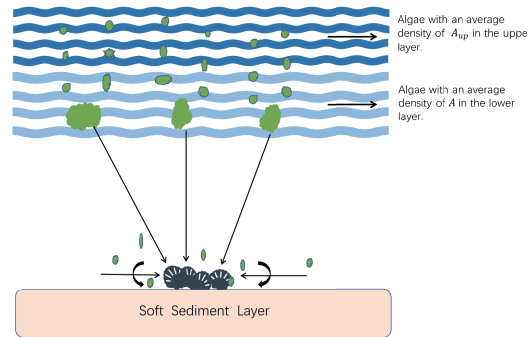
Figure 1. Algae distributes in the lower layer water, the mussel does not only prey on the algae in the local area due to local action, but also may prey on algae in other parts of the space.

In order to depict the non-local predation of the mussel for algae in whole space and at different time, we introduce a nonlocal interaction term into the mussel-algae system proposed by Van de Koppel et al. [23]:

$$\begin{cases} \dfrac{\partial M}{\partial t}=D_M\triangle M+ec(\int_{-\infty}^{t}\int_{R^2}K(x-y,t-s)A(y,s)dsdy)M-d_M\dfrac{k_M}{k_M+M}M, \\ \dfrac{\partial A}{\partial t}=D_A\triangle A+(A_{up}-A)\rho-\dfrac{c}{H}(\int_{-\infty}^{t}\int_{R^2}K(x-y,t-s)A(y,s)dsdy)M, \end{cases}$$

(2.1)

where M is the density of mussel, A is the density of algae, $\triangle=\frac{\partial}{\partial X^2}+\frac{\partial}{\partial Y^2}$ represents Laplace operator of classical random diffusion, e is a conversion constant relating ingested algae to mussel biomass production, c is the consumption constant, d_M is the maximal per capita mussel mortality rate, k_M is the value of mussel at which mortality is half maximal, A_{up} describes the uniform concentration of algae in the upper reservoir water layer, is the rate of exchange between the lower and upper water layers, H is the height of the lower water layer, V is the speed of the tidal current assumed to be acting in the positive X-direction and D_M and D_A are the motility and lateral diffusion coefficients of the mussel and algae.

To analyze the dynamics of the spatial pattern, we transform a two-dimensional system into a three-dimensional reaction-diffusion system by using the method described in literature [5, 7, 9, 11] to deal with nonlocal interaction term. Let

$$V(x,t)=\int_{-\infty}^{t}\int_{R^2}K(x-y,t-s)A(y,s)dsdy,$$

and then system (2.1) is transformed into the following form:

$$\begin{cases} \dfrac{\partial M}{\partial t} = D_M \triangle M + ecVM - d_M \dfrac{k_M}{k_M + M}M, \\ \dfrac{\partial A}{\partial t} = D_A \triangle A + (A_{up} - A)\rho - \dfrac{c}{H}VM, \\ \dfrac{\partial V}{\partial t} = \triangle V + \dfrac{1}{\tau}(A - V). \end{cases} \qquad (2.2)$$

To reduce the parameters and simplify the system, we introduce dimensionless variables and parameters in the system (2.2),

$$(x, y) = (X, Y)\sqrt{\dfrac{\omega}{D_A}}, \qquad s = d_M t, \qquad m = \dfrac{1}{k_M}M, \qquad a = \dfrac{1}{A_{up}}A, \qquad v = \dfrac{1}{A_{up}}V,$$

with $\omega = \dfrac{ck_M}{H}$, and

$$\alpha = \dfrac{\rho}{\omega}, \qquad \beta = \dfrac{d_M}{\omega}, \qquad \gamma = \dfrac{1}{d_M \tau}, \qquad r = \dfrac{ecA_{up}}{d_M}, \qquad \mu_1 = \dfrac{D_M}{\beta D_A}, \qquad u_2 = \dfrac{1}{\beta D_A},$$

the system (2.2) can be rewritten as

$$\begin{cases} \dfrac{\partial m}{\partial t} = \mu_1 \Delta m + rvm - \dfrac{m}{1+m}, \\ \dfrac{\partial a}{\partial t} = \dfrac{1}{\beta}\triangle a + \dfrac{\alpha}{\beta}(1 - a) - \dfrac{1}{\beta}vm, \\ \dfrac{\partial v}{\partial t} = \mu_2 \Delta v + \gamma(a - v). \end{cases} \qquad (2.3)$$

In the system (2.3), all parameters are not less than 0 based on the actual biological significance. Next, we mainly carry out dynamic analysis on system (2.3) to obtain the existence conditions for generating Hopf bifurcation and Turing instability.

3. Dynamic analysis

3.1. Local stability at equilibrium point E_0

When there is no diffusion, the ordinary differential system corresponding to the system (2.3) is

$$\begin{cases} \dfrac{dm}{dt} = rvm - \dfrac{m}{1+m}, \\ \dfrac{da}{dt} = \dfrac{1}{\beta}(1 - a)\alpha - \dfrac{1}{\beta}vm, \\ \dfrac{dv}{dt} = \gamma(a - v). \end{cases} \qquad (3.1)$$

We get two equilibrium points of system (3.1): $E_0 = (0, 1, 1)$, $E^* = (m^*, a^*, v^*) = (\alpha\frac{r-1}{1-\alpha r}, \frac{1-\alpha r}{r(1-\alpha)}, \frac{1-\alpha r}{r(1-\alpha)})$, where E_0 represents exposed coastal rocks without mussels, and the equilibrium point E^* is the coexistence of the mussel and the algae. From a biological point of view, the densities of the mussel and the algae cannot be

negative. Therefore, if the condition (J_1) $0 < \alpha < 1$ and $1 < r < \frac{1}{\alpha}$; or (J_2) $\alpha > 1$ and $\frac{1}{\alpha} < r < 1$ is satisfied, the m^*, a^*, v^* are all greater than 0. Then, we know that E^* is a positive equilibrium point.

Next, we analyze the local stabilities of equilibrium points E_0 and E^*. The *Jacobian* matrix at E_0 is

$$J_{E_0} = \begin{pmatrix} r - 1 & 0 & 0 \\ -\frac{1}{\beta} & -\frac{1}{\beta} & 0 \\ 0 & \gamma & -\gamma \end{pmatrix}.$$

The characteristic equation corresponding to this matrix is

$$(\lambda - r + 1)(\lambda + \frac{1}{\beta})(\lambda + \gamma) = 0.$$

We get the characteristic roots $\lambda_1 = r - 1$, $\lambda_2 = -\frac{1}{\beta}$ and $\lambda_3 = -\gamma$, only when the condition J_2 is satisfied, all eigenvalues have negative real parts. Then, E_0 is locally asymptotically stable. However, E_0 becomes unstable when J_1 is satisfied. According to the actual biological meaningful, the study is more meaningful, when E_0 becomes unstable. Then, we mainly analyze the condition J_1.

3.2. Local stability at equilibrium point E^*

For the system (2.3), we can get the linearized model at equilibrium point E^* as follows:

$$\begin{cases} \dfrac{\partial m}{\partial t} = b_{11}m + b_{12}a + b_{13}v + \mu_1 \triangle m, \\ \dfrac{\partial a}{\partial t} = b_{21}m + b_{22}a + b_{23}v + \dfrac{1}{\beta}\triangle a, \\ \dfrac{\partial v}{\partial t} = b_{31}m + b_{32}a + b_{33}v + \mu_2 \triangle v, \end{cases} \tag{3.2}$$

where

$$b_{11} = \frac{(1 - \alpha r)\alpha(r - 1)}{(1 - \alpha)^2}, \qquad b_{12} = 0, \qquad b_{13} = \frac{\alpha r(r - 1)}{1 - \alpha r},$$

$$b_{21} = -\frac{1 - \alpha r}{\beta r(1 - \alpha)}, \qquad b_{22} = -\frac{\alpha}{\beta}, \qquad b_{23} = -\frac{\alpha(r - 1)}{\beta(1 - \alpha r)},$$

$$b_{31} = 0, \qquad\qquad\qquad b_{32} = \gamma, \qquad b_{33} = -\gamma.$$

Next, we analyze the spatiotemporal dynamic behavior of system (3.2) by conducting nonuniform perturbations at equilibrium point E^*:

$$\begin{pmatrix} m \\ a \\ v \end{pmatrix} = \begin{pmatrix} m^* \\ a^* \\ v^* \end{pmatrix} + \varepsilon \begin{pmatrix} C_k^1 \\ C_k^2 \\ C_k^3 \end{pmatrix} exp(\lambda t + i\overrightarrow{\kappa} \cdot \overrightarrow{\zeta}) + c.c. + o(\varepsilon^2), \tag{3.3}$$

where λ is the growth rate of perturbations in time t, i is the imaginary unit satisfying $i^2 = -1$, $\kappa_x \cdot \kappa_y = k^2$ and k is the wave number (k may not be an

integer), $\zeta = (x, y)$ is the spatial vector in two dimensions. Then, we can obtain the characteristic equation:

$$\begin{vmatrix} b_{11} - \mu_1 k^2 - \lambda & b_{12} & b_{13} \\ b_{21} & b_{22} - \frac{1}{\beta} k^2 - \lambda & b_{23} \\ b_{31} & b_{32} & b_{33} - \mu_2 k^2 - \lambda \end{vmatrix} = 0, \quad (3.4)$$

which is equivalent to

$$\lambda^3 + b_1(k)\lambda^2 + b_2(k)\lambda + b_3(k) = 0, \quad (3.5)$$

with

$$b_1(k) = (\mu_1 + \frac{1}{\beta} + \mu_2)k^2 + \frac{\alpha}{(\alpha - 1)^2}(\alpha r^2 + \alpha\gamma - \alpha r + \frac{\alpha^2}{\beta} - 2\gamma - r - \frac{2\alpha^2}{\beta}$$
$$+ \frac{1}{\beta} + 1 + \frac{\gamma}{\alpha}),$$

$$b_2(k) = \frac{(\beta\mu_1\mu_2 + \mu_1 + \mu_2)}{\beta}k^4 + \frac{1}{\beta(\alpha - 1)^2}(\alpha^2\beta\mu_2 r^2 + \alpha^2\beta\gamma\mu_1 - \alpha^2\beta\mu_2 r + \alpha^3 mu_1$$
$$+ \alpha^3 mu_2 + \alpha^2 r^2 - 2\alpha\beta\gamma\mu_1 - \alpha\beta\mu_2 r + \alpha^2\gamma - 2\alpha^2\mu_1 - 2\alpha^2\mu_2 - \alpha^2 r + \alpha\beta\mu_2$$
$$+ \beta\gamma\mu_1 - \alpha r + \gamma + \alpha\mu_1 + \alpha\mu_2 + \alpha - 2\alpha\gamma)k^2 + \frac{\alpha}{(\alpha - 1)^2\beta(\alpha r - 1)}(\alpha^2\beta\gamma r^3$$
$$+ \alpha^3 r^3 - \alpha^2\beta\gamma r^2 - \alpha + \alpha^3\gamma r - \alpha^3 r^2 - 2\alpha\beta\gamma r^2 - 3\alpha^2\gamma r - 2\alpha^2 r^2 + 2\alpha\beta\gamma r$$
$$+ 2\alpha^2 r + 3\alpha\gamma r + \beta\gamma r + \alpha r - \beta\gamma - \gamma r),$$

$$b_3(k) = \frac{\mu_1\mu_2}{\beta}k^6 + \frac{1}{\beta(\alpha - 1)^2}(\alpha^3\mu_1\mu_2 + \alpha^2\mu_2 r^2 + \alpha^2\mu_1\gamma - 2\alpha^2\mu_1\mu_2 - \alpha^2\mu_2 r - \gamma$$
$$- 2\alpha\gamma\mu_1 + \alpha\mu_1\mu_2 - \alpha\mu_2 r + \alpha\mu_2 + \mu_1\gamma)k^4 + \frac{\alpha}{(\alpha - 1)^2\beta(\alpha r - 1)}(\alpha^3 r_3\mu_2$$
$$+ \alpha^3\gamma\mu_1 r - \alpha^3\mu_2 r_2 + \alpha^2\gamma r^3 - 3\alpha^2\gamma\mu_1 r - alpha^2 r^2\gamma - 2\alpha^2\mu_2 r^2 - \alpha\mu_2 + \gamma r$$
$$+ 3\alpha\gamma\mu_1 r - 2\alpha\gamma r^2 + 2\alpha\gamma r + \alpha\mu_2 r - \gamma\mu_1 r + 2\alpha^2\mu_2 r)k^2 + \frac{\gamma\alpha(r - 1)(\alpha r - 1)}{\beta(\alpha - 1)}.$$

Further, we can give

$$b_1(k) \cdot b_2(k) - b_3(k) = y_3 k^6 + y_2 k^4 + y_1 k^2 + y_0,$$

where

$$y_3 = \frac{(\mu_1 + \mu_2)(\beta\mu_2 + 1)(\beta\mu_1 + 1)}{\beta^2},$$

$$y_2 = \frac{1}{\beta^2(\alpha - 1)^2}(2\alpha^2\beta^2\mu_1\mu_2 r^2 + \alpha^2\beta^2\mu_2^2 r^2 + \alpha^2\beta^2\gamma\mu_1^2 + 2\alpha^2\beta^2\gamma\mu_1\mu_2 - 2\alpha^2\beta^2\mu_1\mu_2 r$$
$$- \alpha r + \alpha + 2\alpha^3\beta\mu_1^2 + \alpha^3\beta\mu_2^2 + 2\alpha^2\beta\mu_1 r^2 + 2\alpha^2\beta\mu_2 r^2 - 2\alpha\beta^2\gamma\mu_1^2 + \alpha^3\beta\mu_1^2$$
$$- 2\alpha\beta^2\mu_1\mu_2 r + \gamma - \alpha\beta^2\mu_2^2 r + 2\alpha^2\beta\gamma\mu_1 + 2\alpha^2\beta\gamma\mu_2 - 2\alpha^2\beta - 4\alpha^2\beta\mu_1\mu_2$$
$$- 2\alpha^2\beta\mu_1 r - 2\alpha^2\beta\mu_2^2 - 2\alpha^2\beta\mu_2 r + 2\alpha\beta^2\mu_1\mu_2 + \alpha\beta^2\mu_2^2 + \beta^2\gamma\mu_1^2 + 2\beta^2\gamma\mu_1\mu_2$$
$$+ 2\alpha^3\mu_1 + 2\alpha^3\mu_2 + \alpha^2 r^2 - 4\alpha\beta\gamma\mu_1 - 2\alpha\gamma - 4\alpha\beta\gamma\mu_2 + \alpha\beta\mu_1^2 + 2\alpha\beta\mu_1\mu_2$$

$$+ 2\alpha\mu_1 + \alpha\beta\mu_2^2 - 2\alpha\beta\mu_2 r + \alpha^2\gamma - 4\alpha^2\mu_1 - 4\alpha^2\mu_2 - r\alpha^2 + 2\alpha\beta\mu_1 + 2\alpha\beta\mu_2$$
$$+ 2\beta\gamma\mu_1 + 2\beta\gamma\mu_2 - 2\alpha\beta\mu_1 r + 2\alpha\mu_2 - \alpha^2\beta^2\mu_2^2 r - 4\alpha\beta^2\gamma\mu_1\mu_2),$$

$$y_1 = \frac{1}{\beta^2(\alpha-1)^4(\alpha r-1)}(r(\mu_1+\mu_2)\alpha^7 + (2r(r^2+\gamma-r)(\mu_1+\mu_2)\beta - 2r^2 + (-4\mu_1$$
$$- 4\mu_2 + 2\gamma)r + 2r^3 - \mu_1 - \mu_2)\alpha^6 + ((\alpha^4\mu_2 - 2r^3\mu_2 + ((2\mu_1+\mu_2)\gamma + \mu_2)r^2$$
$$- 2\gamma(\mu_1+\mu_2)r + \mu_1\gamma^2)r\beta^2 + (r^5 - 2r^4 + (-4\mu_1 - 4\mu_2 + 2\gamma + 1)r^3 - 2r^2\gamma$$
$$+ (\gamma^2 + (-8\mu_1 - 9\mu_2)\gamma + 4\mu_1 + 4\mu_2)r - 2\gamma(\mu_1 + \tfrac{1}{2}\mu_2))\beta - 4r^3 + (6\mu_1 + 6\mu_2$$
$$- 9\gamma + 4)r + 4\mu_1 + 4\mu_2 - \gamma)\alpha^5 + ((-3r^4\mu_2 + ((-4\mu_1 - 4\mu_2)\gamma + 6\mu_2)r^3 - 3\mu_2 r^2$$
$$- 4\gamma(\mu_1\gamma - \mu_1 - \mu_2)r - \mu_1\gamma^2)\beta^2 + (-3r^4 + (2\mu_1 + 2\mu_2 - 4\gamma + 6)r^3 + (6\mu_1$$
$$+ 6\mu_2 - 3)r^2 + (-4\gamma^2 + (12\mu_1 + 16\mu_2 + 4)\gamma - 6\mu_1 - 6\mu_2)r - \gamma^2 + (8\mu_1 + 4\mu_2)\gamma$$
$$- 2\mu_1 - 2\mu_2)\beta + 2r^3 + 6r^2 + (-4\mu_1 - 4\mu_2 + 16\gamma - 6)r - 6\mu_1 - 6\mu_2 + 4\gamma - 2)\alpha^4$$
$$+ ((((2\mu_1 + 2\mu_2)\gamma + 3\mu_2)r^3 + ((6\mu_1 + 6\mu_2)\gamma - 6\mu_2)r^2 + (6\mu_1\gamma^2 + 3\mu_2 + (-6\mu_1$$
$$- 6\mu_2)\gamma)r + 4\gamma(\mu_1\gamma - \tfrac{1}{2}\mu_1 - \tfrac{1}{2}\mu_2))\beta^2 + ((2\gamma + 3)r^3 + (-4\mu_1 - 4\mu_2 + 6\gamma - 6)r^2$$
$$+ (3 + 6\gamma^2 + (-8\mu_1 - 14\mu_2 - 6)\gamma)r + 4\gamma^2 + (-12\mu_1 - 6\mu_2 - 2)\gamma + 4\mu_1 + 4\mu_2)\beta$$
$$- 4r^2 + (\mu_1 + \mu_2 - 14\gamma)r + 4\mu_1 + 4\mu_2 - 6\gamma + 4)\alpha^3 + (((((-4\mu_1 - 4\mu_2)\gamma - \mu_2)r^2$$
$$+ (-4\mu_1\gamma^2 + 2\mu_2)r - 6\mu_1\gamma^2 + (4\mu_1 + 4\mu_2)\gamma - \mu_2)\beta^2 + ((-4\gamma - 1)r^2 + (-4\gamma^2$$
$$+ (2\mu_1 + 6\mu_2)\gamma + 2\mu_1 + 2\mu_2 + 2)r - 6\gamma^2 + (8\mu_1 + 4\mu_2 + 4)\gamma - 2\mu_1 - 2\mu_2 - 1)\beta$$
$$+ (6\gamma + 2)r - \mu_1 - \mu_2 + 4\gamma - 2)\alpha^2 + (((\mu_1\gamma + 2\mu_1 + 2\mu_2)r + 4\mu_1\gamma - 2\mu_1$$
$$- 2\mu_2)\beta^2 + ((-\mu_2 + \gamma + 2)r - 2\mu_1 - \mu_2 + 4\gamma - 2)\beta - r - 1)\gamma\alpha - \beta\gamma^2(\beta\mu_1 + 1)),$$

$$y_0 = h_2\gamma^2 + h_1\gamma + h_0,$$

with

$$h_2 = \frac{\alpha}{\beta(\alpha-1)^4(\alpha r-1)}(\alpha^4\beta r^3 - \alpha^4\beta r^2 - 2\alpha^3\beta r^3 + \alpha^5 r + \alpha^2\beta r^3 - 5\alpha^4 r$$
$$+ 2\alpha^3\beta r + 3\alpha^2\beta r^2 + 10\alpha^3 r - 3\alpha^2\beta r - 2\alpha\beta r^2 - \alpha^2\beta - 10\alpha^2 r + 2\alpha\beta$$
$$+ 5\alpha r + \beta^2 r - \beta^2 - \beta r),$$

$$h_1 = \frac{\alpha}{\beta^2(\alpha-1)^4(\alpha r-1)}(\alpha^4\beta^2 r^5 - 2\alpha^4\beta^2 r^4 + 2\alpha^5\beta r^3 + \alpha^4\beta^2 r^3 - 3\alpha^3\beta^2 r^4 - 2\alpha^5\beta r^2$$
$$+ 6\alpha^6 r - 4\alpha^4\beta r^3 + 6\alpha^3\beta^2 r^3 + \alpha^4\beta r^2 - 3\alpha^3\beta^2 r^2 + 2\alpha^3\beta r^3 + 3\alpha^2\beta^2 r^3 - 5\alpha^5 r$$
$$+ 3\alpha^4\beta r - \alpha\beta^2 - 6\alpha^2\beta^2 r^2 + 10\alpha^4 r - 4\alpha^3\beta r + 3\alpha^2\beta^2 r - \alpha^2\beta r^2 - \alpha\beta^2 r^2 - \alpha^3\beta$$
$$- 10\alpha^3 r + 2\alpha\beta^2 r + \beta r + \alpha^2\beta + 5\alpha^2 r + 3\alpha^3\beta r^2 + \alpha\beta - \alpha r - \alpha\beta r^2 - \beta),$$

$$h_0 = \frac{\alpha}{\beta^2(\alpha-1)^4(\alpha r-1)}(\alpha^5\beta r^5 - 2\alpha^5\beta r^4 + \alpha^6 r^3 + \alpha^5\beta r^3 - 3\alpha^4\beta r^4 - \alpha^6 r^2 - 2\alpha^5 r^3$$
$$+ \alpha^2 r + \alpha^4 r^3 + \alpha^3\beta r^3 + 2\alpha^4 r + 3\alpha^4 r^2 - 6\alpha^3\beta r^2 - 3\alpha^4 r + 3\alpha^5\beta r - 2\alpha^3 r^2$$
$$- \alpha^2\beta r^2 - \alpha^2\beta + 6\alpha^4\beta r^3 - 3\alpha^4\beta r^2 - \alpha^2 - \alpha^4 + 2\alpha^2\beta r + 2\alpha^3).$$

It can be drawn from the practical biological significance of the parameters: $y_3 > 0$.

When we don't consider space diffusion, namely $k = 0$, we can get

$$b_1(0) = \frac{1}{\beta(\alpha-1)^2}((\alpha^2\beta - 2\alpha\beta + \beta)\gamma + \alpha^3 - 2\alpha^2 + (r^2 - r)\beta\alpha^2 + (1 + (-r + 1)\beta)\alpha),$$

$$b_2(0) = \frac{\alpha}{(\alpha-1)^2\beta(\alpha r - 1)}(\alpha^2\beta\gamma r^3 + \alpha^3 r^3 - \alpha^2\beta\gamma r^2 + \alpha^3\gamma r - \alpha^3 r^2 - 2\alpha\beta\gamma r^2$$
$$- 3\alpha^2\gamma r - \alpha + 2\alpha^2 r + 3\alpha\gamma r + \beta\gamma r + \alpha r - \beta\gamma - \gamma r - 2\alpha^2 r^2 + 2\alpha\beta\gamma r),$$

$$b_3(0) = \frac{\alpha(\alpha r - 1)(r - 1)\gamma}{\beta(\alpha-1)}.$$

Let $f(k) = b_1(k) \cdot b_2(k) - b_3(k)$, and then we can get: $f(0) = b_1(0) \cdot b_2(0) - b_3(0) = y_0$.

Next, we analyze the local stability at the coexistence equilibrium point E^* of system (3.1). Through calculation, the corresponding characteristic equation of the *Jacobian* matrix at E^* is:

$$\lambda^3 + b_1(0)\lambda^2 + b_2(0)\lambda + b_3(0) = 0.$$

Theorem 3.1. *For the system* (3.1), *if*
(H_1) $(\alpha^2\beta - 2\alpha\beta + \beta)\gamma + \alpha^3 - 2\alpha^2 + (r^2 - r)\beta\alpha^2 + (1 + (-r + 1)\beta)\alpha > 0$; *or*
(H_2) (i) $h_2 > 0$, $h_1 > 0$, $h_0 > 0$, $h_1^2 - 4h_2 h_0 > 0$, *and* $\gamma \in (0, +\infty)$; *or*

(ii) $h_2 > 0$, $h_0 < 0$, *and* $\gamma \in \left(\frac{-h_1 + \sqrt{h_1^2 - 4h_2 h_0}}{2h_2}, +\infty\right)$; *or*
(iii) $h_2 > 0$, $h_1 < 0$, $h_0 > 0$, $h_1^2 - 4h_2 h_0 > 0$, *and*
$\gamma \in \left(0, \frac{-h_1 - \sqrt{h_1^2 - 4h_2 h_0}}{2h_2}\right) \cup \left(\frac{-h_1 + \sqrt{h_1^2 - 4h_2 h_0}}{2h_2}, +\infty\right)$;*or*
(iv) $h_2 > 0$, $h_0 > 0$, $h_1^2 - 4h_2 h_0 < 0$ *and* $\gamma \in (0, +\infty)$; *or*
(v) $h_2 > 0$, $h_0 > 0$, $h_1^2 - 4h_2 h_0 = 0$ *and* $\gamma \in \left(0, -\frac{h_1}{2h_2}\right) \cup \left(-\frac{h_1}{2h_2}, +\infty\right)$; *or*

(vi) $h_2 < 0$, $h_0 > 0$, $\gamma \in \left(0, \frac{-h_1 + \sqrt{h_1^2 - 4h_2 h_0}}{2h_2}\right)$; *or*

(vii) $h_2 < 0$, $h_0 < 0$, $h_1^2 - 4h_2 h_0 > 0$, *and* $\gamma \in \left(\frac{-h_1 - \sqrt{h_1^2 - 4h_2 h_0}}{2h_2}, \frac{-h_1 + \sqrt{h_1^2 - 4h_2 h_0}}{2h_2}\right)$; *or*

both of the above two conditions H_1 and H_2 are true, then the coexistence equilibrium point E^* of system (3.1) *is locally asymptotically stable.*

Proof. From H_1, we can get $b_1(0) > 0$, and from the conditions of the existence of E^*, we know $b_3(0) > 0$. However, the sign of $f(0)$ is uncertain. Then, we mainly discuss the sign of $f(0)$ in the following:

(i) If $h_2 > 0$, $h_1 > 0$ and $h_0 > 0$ hold, it is easy to get $f(0) > 0$ for any $\gamma > 0$ (see Figure 2(a));

Suppose that the roots of the quadratic function $f(0) = 0$ are $\gamma_1 = \frac{-h_1 + \sqrt{h_1^2 - 4h_2 h_0}}{2h_2}$ and $\gamma_2 = \frac{-h_1 - \sqrt{h_1^2 - 4h_2 h_0}}{2h_2}$.

(ii) From the second condition in H_2, we know $\sqrt{h_1^2 - 4h_2 h_0} > |h_1|$, and then $\gamma_2 < 0 < \gamma_1$ is obtained. Therefore, we get $f(0) > 0$ because of $h_0 < 0$ and $\gamma > \gamma_1$ (see Figure 2(b)).

(iii) From the third condition in H_2, we know $0 < \gamma_2 < \gamma_1$. According to the properties of quadratic function, we get $f(0) > 0$, when $\gamma \in \left(0, \frac{-h_1 - \sqrt{h_1^2 - 4h_2 h_0}}{2h_2}\right) \cup \left(\frac{-h_1 + \sqrt{h_1^2 - 4h_2 h_0}}{2h_2}, +\infty\right)$ (see Figure 2(c)).

(iv) From the fourth condition in H_2, we know $\gamma_1 = \gamma_2 = -\frac{h_1}{2h_2}$. Based on $h_0 > 0$, we get $f(0) > 0$, when $\gamma \in (0, -\frac{h_1}{2h_2}) \cup (-\frac{h_1}{2h_2}, +\infty)$ (see Figure 2(d)).

(v) From the fifth condition in H_2, there is no intersection point between quadratic function $f(0)$ and x-axis. Then, $f(0) > 0$ holds for $\gamma > 0$ because of $h_0 > 0$ (see Figure 2(e)).

(vi) From the sixth condition in H_2, we can give $\sqrt{h_1^2 - 4h_2h_0} > |h_1|$, which means $\gamma_2 < 0 < \gamma_1$. Therefore, when $\gamma \in (0, \frac{-h_1 + \sqrt{h_1^2 - 4h_2h_0}}{2h_2})$, we get $f(0) > 0$ due to $h_0 > 0$ (see Figure 2(f)).

(vii) From the seventh condition in H_2, we get $0 < \gamma_2 < \gamma_1$. Therefore, when $\gamma \in (\frac{-h_1 - \sqrt{h_1^2 - 4h_2h_0}}{2h_2}, \frac{-h_1 + \sqrt{h_1^2 - 4h_2h_0}}{2h_2})$, we get $f(0) > 0$ because of $h_0 < 0$ (see Figure 2(g)).

Through the above analysis, as long as one condition in H_2 holds, one can obtain $f(0) > 0$. Then, E_* of system (3.1) is locally asymptotically stable based on the $Routh - Hurwitz$ criterion. $\square$
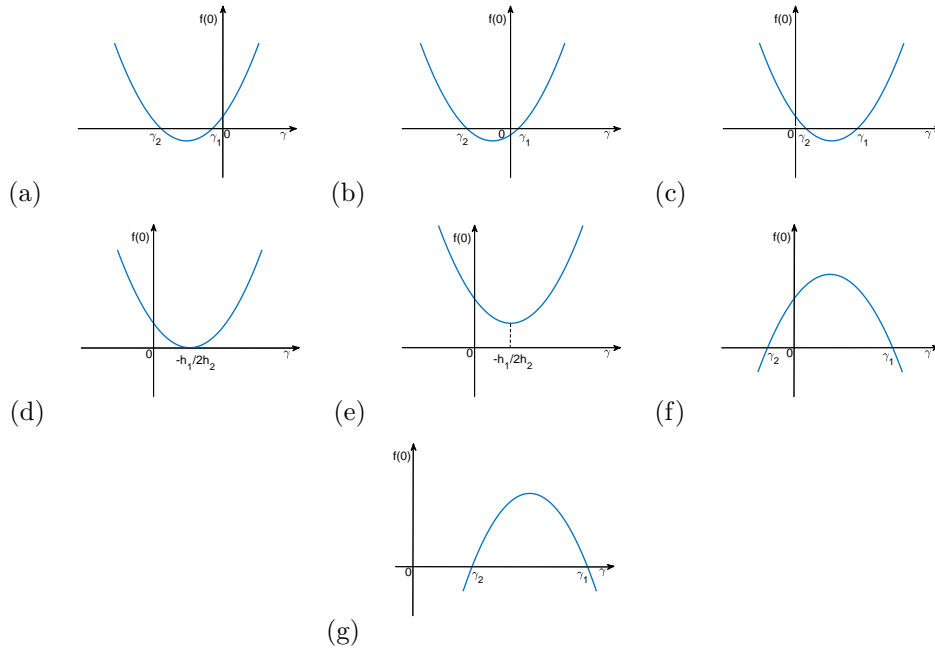
Figure 2. Schematic diagrams of the quadratic function $f(0)$ in Theorem 3.1: (a) $h_2 > 0$, $h_1 > 0$, $h_0 > 0$, $h_1^2 - 4h_2h_0 > 0$; (b) $h_2 > 0$, $h_0 < 0$; (c) $h_2 > 0$, $h_1 < 0$, $h_0 > 0$, $h_1^2 - 4h_2h_0 > 0$; (d) $h_2 > 0$, $h_0 > 0$, $h_1^2 - 4h_2h_0 = 0$; (e) $h_2 > 0$, $h_0 > 0$, $h_1^2 - 4h_2h_0 < 0$; (f) $h_2 < 0$, $h_0 > 0$; (g) $h_2 < 0$, $h_0 < 0$, $h_1^2 - 4h_2h_0 > 0$.

3.3. Conditions for the generation of Hopf bifurcation and Turing instability

Theorem 3.2. *When system* (3.1) *satisfies both of the following conditions:*
(H_1) $(\alpha^2\beta - 2\alpha\beta + \beta)\gamma + \alpha^3 - 2\alpha^2 - (r^2 - r)\beta\alpha^2 + (1 + (-r + 1)\beta)\alpha > 0$;
$(H_3) : h_2\gamma^2 + h_1\gamma + h_0 = 0$;

then system (3.1) *undergoes Hopf bifurcation at the coexistence equilibrium point* E^*.

Proof. $b_3(0) = \frac{\gamma\alpha(r-1)(\alpha r-1)}{\beta(\alpha-1)} > 0$ holds due to the conditions for the existence of E^*. If condition H_1 holds, then $b_1(0) > 0$. From condition H_3, we can get $f(0) = 0$. According to the theorem in literature [9, 17], when $b_1(0) > 0$, $b_3(0) > 0$ and $f(0) = 0$ are satisfied, the Hopf bifurcation can be generated at E^* for system (3.1). □

Meanwhile, we can get the critical bifurcation line H: $f_0 = h_2\gamma^2 + h_1\gamma + h_0 = 0$.

Next, we study the influence of space diffusion on the coexistence equilibrium point E^* of system (3.2). According to the condition of local stability in Theorem 3.1, then $b_1(k) = (\mu_1 + \frac{1}{\beta} + \mu_2)k^2 + b_1(0) > 0$ holds. However, the signs of $b_3(k)$ and $f(k)$ are uncertain. Then, we analyze these two expressions in the following.

Let $z = k^2$ and $F_1(z) = b_3(k)$, and then

$$F_1(z) = f_3 z^3 + f_2 z^2 + f_1 z + f_0, \tag{3.6}$$

where

$$f_3 = \frac{1}{\beta}\mu_1\mu_2,$$

$$f_2 = \frac{1}{\beta(\alpha-1)^2}(\alpha^3\mu_1\mu_2 + \alpha^2\mu_2 r^2 + \alpha^2\mu_1\gamma - 2\alpha^2\mu_1\mu_2 - \alpha^2\mu_2 r - 2\alpha\gamma\mu_1 + \alpha\mu_1\mu_2 - \alpha\mu_2 r$$
$$+ \alpha\mu_2 + \mu_1\gamma),$$

$$f_1 = \frac{\alpha}{(\alpha-1)^2\beta(\alpha r-1)}(\alpha^3 r_3\mu_2 + \alpha^3\gamma\mu_1 r - \alpha^3\mu_2 r_2 + \alpha^2\gamma r^3 - 3\alpha^2\gamma\mu_1 r - \alpha^2 r^2\gamma - 2\alpha^2\mu_2 r^2$$
$$+ 2\alpha^2\mu_2 r + 3\alpha\gamma\mu_1 r - 2\alpha\gamma r^2 + 2\alpha\gamma r + \alpha\mu_2 r - \gamma\mu_1 r - \alpha\mu_2 + \gamma r - \gamma),$$

$$f_0 = \frac{\gamma\alpha(r-1)(\alpha r-1)}{\beta(\alpha-1)}.$$

Theorem 3.3. *If condition*
(H_4): $f_1 < 0$, *and* $27f_0 f_3^2 + 6f_1 f_3\delta + f_2^3 - 9f_1 f_2 f_3 - 2\delta < 0$; *or*
$f_1 > 0$, $f_2 < 0$, $f_2^2 - 3f_3 f_1 > 0$, *and* $27f_0 f_3^2 + 6f_1 f_3\delta + f_2^3 - 9f_1 f_2 f_3 - 2\delta < 0$; *or*
$f_1 = 0$, $f_2 < 0$, *and* $27f_0 f_3^2 + 6f_1 f_3\delta + f_2^3 - 9f_1 f_2 f_3 - 2\delta < 0$;
is satisfied, then there exists some k, *so that the coexistence equilibrium point* E^* *of system (3.2) is unstable.*

Proof. It is easy to get $f_3 > 0$ and $f_0 > 0$, so is for the cubic function $F_1(z)$, we know $\lim_{z\to\infty} F_1(z) = +\infty$. We can calculate the first order derivative of the $F_1(z)$: $\frac{dF_1(z)}{dz} = 3f_3 z^2 + 2f_2 z + f_1$. Then, the two extreme points of $F_1(z)$ are

$$z_{11} = \frac{-f_2 + \delta}{3f_3}, \quad z_{12} = \frac{-f_2 - \delta}{3f_3}, \quad (\delta = \sqrt{f_2^2 - 3f_3 f_1}), \quad z_{11} > z_{12},$$

(i) if $f_1 < 0$ holds, then we can get $z_{11} > 0 > z_{12}$. $f_0 > 0$ and $27f_0 f_3^2 + 6f_1 f_3\delta + f_2^3 - 9f_1 f_2 f_3 - 2\delta < 0$ indicate $F_1(0) = f_0 > 0$ and $F_1(z_{11}) < 0$ respectively (see Figure 3(a));
(ii) if $f_1 > 0$, $f_2 < 0$ and $f_2^2 - f_3 f_1 > 0$, it is easy to derive $z_{11} > z_{12} > 0$. $f_0 > 0$ and $27f_0 f_3^2 + 6f_1 f_3\delta + f_2^3 - 9f_1 f_2 f_3 - 2\delta < 0$ hold, which shows $F_1(0) = f_0 > 0$ and $F_1(z_{11}) < 0$ (see Figure 3(b));

(iii) if $f_1 = 0$, $f_2 < 0$, and then $z_{11} > z_{12} = 0$ holds. Moreover, the expressions $f_0 > 0$ and $27f_0 f_3^2 + 6f_1 f_3 \delta + f_2^3 - 9f_1 f_2 f_3 - 2\delta < 0$ are satisfied, which indicates $F_1(0) = f_0 > 0$ and $F_1(z_{11}) < 0$ (see Figure 3(c)).

The above analysis shows that z_{11} is the minimum point of $F_1(z)$, and then we can obtain $F_1(z) < 0$ for some $z > 0$, which indicates that $b_3(k) < 0$ for some k. According to the $Routh - Hurwitz$ criterion, E^* of system (3.2) becomes unstable for some k. □
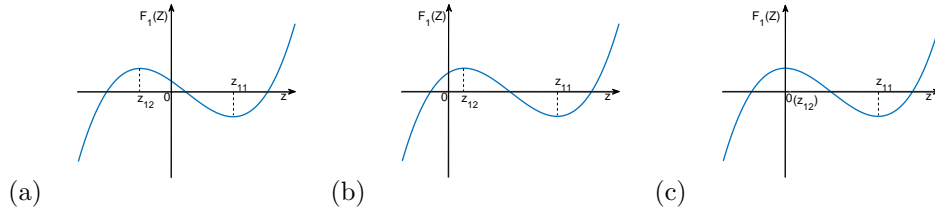
Figure 3. Schematic diagram of the cubic function $F(z)$ ($f_{13} > 0$ and $f_{10} > 0$). (a) $f_{11} < 0$; (b) $f_1 > 0$, and $f_2 < 0$; (c) $f_1 = 0$, and $f_2 < 0$.
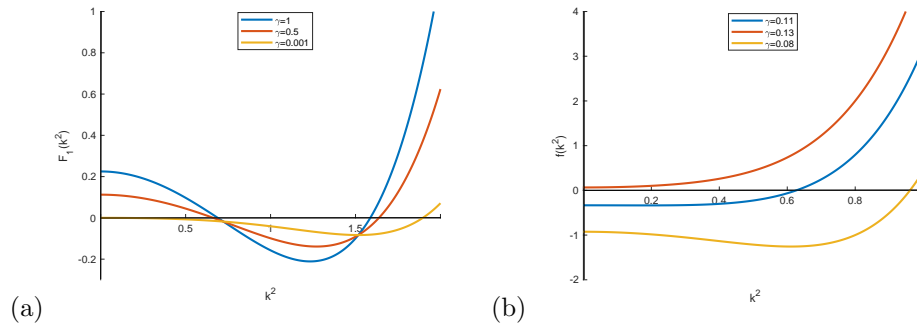
Figure 4. The relationship between the coefficient of the characteristic equation (3.5) and the square of the wave number k^2. For the Figure (a), the parameters we select are: $\alpha = \frac{2}{3}$, $\beta = \frac{2}{15}$, $r = 1.05$, $\mu_1 = 0.025$ and $\mu_2 = 0.05$. For the Figure (b), the parameters we select are: $\alpha = \frac{4}{5}$, $\beta = \frac{1}{5}$, $r = 1.05$, $\mu_1 = 0.025$ and $\mu_2 = 0.05$.

In Figure 4, the relationship between the characteristic equation (3.5) and the square of the wave number k^2 is depicted. As is seen in Figures $4(a)$ and $4(b)$, there exist $k^2 > 0$, making $b_3(k) < 0$ and $b_1(k) \cdot b_2(k) - b_3(k) < 0$.

Now, we consider the sign of $f(k) = b_1(k)b_2(k) - b_3(k)$. Let $e = k^2$, and then

$$f(e) = y_3 e^3 + y_2 e^2 + y_1 e + y_0.$$

It is obvious that $y_3 = \frac{(\mu_1+\mu_2)(\beta\mu_2+1)(\beta\mu_1+1)}{\beta^2} > 0$. Based on condition H_2 in Theorem 3.1, one can obtain $y_0 > 0$.

Theorem 3.4. *If condition*
(H_5) $y_1 < 0$, *and* $27y_0 y_3^2 + 6y_1 y_3 \sqrt{y_2^2 - 3y_1 y_3} + y_2^3 - 9y_1 y_2 y_3 - 2\sqrt{y_2^2 + 3y_1 y_3} < 0$;
or
$y_1 > 0$, $y_2 < 0$, $y_2^2 - y_3 y_1 > 0$ *and* $27y_0 y_3^2 + 6y_1 y_3 \sqrt{y_2^2 - 3y_1 y_3} + y_2^3 - 9y_1 y_2 y_3 - 2\sqrt{y_2^2 + 3y_1 y_3} < 0$; *or*

$y_1 = 0$, $y_2 < 0$, and $27y_0 y_3^2 + 6y_1 y_3 \sqrt{y_2^2 - 3y_1 y_3} + y_2^3 - 9y_1 y_2 y_3 - 2\sqrt{y_2^2 + 3y_1 y_3} < 0$; *is true, then the coexistence equilibrium point E^* of system (3.2) lose stability for some k.*

Through some analysis, we know that $b_3(k)$ and $f(k)$ satisfy similar conditions and structures. Therefore, the proof of the Theorem 3.4 is similar to that of Theorem 3.3, and the reader can verify it by yourself. According to the above analysis, we give the Turing bifurcation line:

$$27f_0 f_3^2 + 6f_1 f_3 \sqrt{f_2^2 - 3f_1 f_3} + f_2^3 - 9f_1 f_2 f_3 - 2\sqrt{f_2^2 + 3f_1 f_3} = 0;$$

or

$$27y_0 y_3^2 + 6y_1 y_3 \sqrt{y_2^2 - 3y_1 y_3} + y_2^3 - 9y_1 y_2 y_3 - 2\sqrt{y_2^2 + 3y_1 y_3} = 0.$$

In summary, the conditions for system (3.2) to give rise to Turing instability are:

$$\begin{cases} H_1 \quad and \quad H_2, \\ H_4 \quad or \quad H_5. \end{cases} \tag{3.7}$$

4. Nonlinear analysis

In this section, we apply the multi-scale analysis method to obtain the amplitude equation based on the following three assumptions for the spatiotemporal dynamic behaviors near the Turing bifurcation point. Assume (1) that the wave vector near the bifurcation point is $|k_j| = k_T$, $j = 1, 2, 3$; (2) the pattern of the system is described by mode of three pairs of wave vectors $(k_j, -k_j)$; (3) the angle of the three pairs of wave vectors is $\frac{2\pi}{3}$ [3,11,16,22]. By calculation, the amplitude equation can be obtained in the following form:

$$\begin{cases} \tau_0 \dfrac{\partial A_1}{\partial t} = \nu A_1 + h\overline{A}_2 \overline{A}_3 - [g_1 |A_1|^2 + g_2(|A_2|^2 + |A_3|^2)]A_1, \\[2mm] \tau_0 \dfrac{\partial A_2}{\partial t} = \nu A_2 + h\overline{A}_1 \overline{A}_3 - [g_1 |A_2|^2 + g_2(|A_1|^2 + |A_3|^2)]A_1, \\[2mm] \tau_0 \dfrac{\partial A_3}{\partial t} = \nu A_3 + h\overline{A}_1 \overline{A}_2 - [g_1 |A_3|^2 + g_2(|A_1|^2 + |A_2|^2)]A_1. \end{cases} \tag{4.1}$$

To consider perturbations of the k around k_T, we need to find the critical wavenumber k_T. The conditions for generating Turing instability are: $I_m(\lambda_k) = 0$ and $R_e(\lambda_k) = 0$ at $k = k_T \neq 0$. For the $b_3(k) = 0$, we get the critical wavenumber $k_T = \sqrt{\frac{-f_2 + \delta}{2f_3}}$, where $\delta = \sqrt{f_2^2 - 3f_3 f_1}$. Then, we derive the critical value γ_T of parameter γ by inserting $k = k_T$ into $b_3(k) = 0$. In the following, we shall give the solution process the amplitude equations. System (2.3) at E^* is rewritten as the following form:

$$\begin{cases} \dfrac{\partial m}{\partial t} = \mu_1 \Delta m + b_{11} m + b_{12} a + b_{13} v + N_1(m, a, v), \\[2mm] \dfrac{\partial a}{\partial t} = \dfrac{1}{\beta} \Delta a + b_{21} m + b_{22} a + b_{23} v + N_2(m, a, v), \\[2mm] \dfrac{\partial v}{\partial t} = \mu_2 \Delta v + b_{21} m + b_{22} a + b_{23} v + N_3(m, a, v), \end{cases} \tag{4.2}$$

where

$$
\begin{cases}
N_1(m, a, v) = \dfrac{(1-\alpha r)^3}{(1-\alpha)^3} m^2 + rvm - \dfrac{(1-\alpha r)^4}{(1-\alpha)^4} m^3, \\[2mm]
N_2(m, a, v) = -\dfrac{1}{\beta} mv, \\[2mm]
N_3(m, a, v) = 0.
\end{cases}
$$

Since near the bifurcation point $\gamma = \gamma_T$, the solution of system (2.3) can be expressed as:

$$
U = \begin{pmatrix} m \\ a \\ v \end{pmatrix} = \Sigma_{i=1}^{3} \begin{pmatrix} A_i^m \\ A_i^a \\ A_i^v \end{pmatrix} exp(i \cdot \overrightarrow{\kappa_i} \cdot \overrightarrow{\zeta}).
$$

Let $U = (m, a, v)^T$, $N = (N_1, N_2, N_3)^T$, the system (4.2) can be rewritten as:

$$
\frac{\partial U}{\partial t} = LU + N(c.c), \tag{4.3}
$$

where

$$
L = \begin{pmatrix}
b_{11} + \mu_1 \Delta & b_{12} & b_{13} \\[1mm]
b_{21} & b_{22} + \frac{1}{\beta} \Delta & b_{23} \\[1mm]
b_{31} & b_{32} & b_{33} + \mu_2 \Delta
\end{pmatrix},
$$

$$
N = \begin{pmatrix}
\frac{(1-\alpha r)^3}{(1-\alpha)^3} m^2 + rmv - \frac{(1-\alpha r)^4}{(1-\alpha)^4} m^3 \\[2mm]
-\frac{mv}{\beta} \\[2mm]
0
\end{pmatrix}.
$$

Let

$$
L = L_T + (\gamma_T - \gamma)M, \tag{4.4}
$$

where

$$
L_T = \begin{pmatrix}
b_{11}^* + \mu_1 \Delta & b_{12}^* & b_{13}^* \\[1mm]
b_{21}^* & b_{22}^* + \frac{1}{\beta} \Delta & b_{23}^* \\[1mm]
b_{31}^* & b_{32}^* & b_{33}^* + \mu_2 \Delta
\end{pmatrix},
$$

$$
M = \begin{pmatrix}
c_{11} & c_{12} & c_{13} \\
c_{21} & c_{22} & c_{231} \\
c_{31} & c_{32} & c_{33}
\end{pmatrix},
$$

and

$$
b_{11}^* = \frac{(1-\alpha r)\alpha(r-1)}{(1-\alpha)^2}, \qquad b_{12}^* = 0, \qquad b_{13}^* = \frac{\alpha r(r-1)}{1-\alpha r},
$$

$$
b_{21}^* = -\frac{1-\alpha r}{\beta r(1-\alpha)}, \qquad b_{22}^* = -\frac{\alpha}{\beta}, \qquad b_{23}^* = -\frac{\alpha(r-1)}{\beta(1-\alpha r)},
$$

$$b_{31}^* = 0, \qquad b_{32}^* = \gamma_T, \qquad b_{33}^* = -\gamma_T,$$

$$c_{11} = \frac{b_{11} - b_{11}^*}{\gamma_T - \gamma}, \qquad c_{12} = \frac{b_{12} - b_{12}^*}{\gamma_T - \gamma}, \qquad c_{13} = \frac{b_{13} - b_{13}^*}{\gamma_T - \gamma},$$

$$c_{21} = \frac{b_{21} - b_{21}^*}{\gamma_T - \gamma}, \qquad c_{22} = \frac{b_{22} - b_{22}^*}{\gamma_T - \gamma}, \qquad c_{23} = \frac{b_{23} - b_{23}^*}{\gamma_T - \gamma},$$

$$c_{31} = \frac{b_{31} - b_{31}^*}{\gamma_T - \gamma}, \qquad c_{32} = \frac{b_{32} - b_{32}^*}{\gamma_T - \gamma}, \qquad c_{33} = \frac{b_{33} - b_{33}^*}{\gamma_T - \gamma}.$$

For using the multiple scale analysis, let

$$\gamma_T - \gamma = \varepsilon\gamma_1 + \varepsilon^2\gamma_2 + \varepsilon^3\gamma_3 + o(\varepsilon^4), \tag{4.5}$$

$$U = \begin{pmatrix} m \\ a \\ v \end{pmatrix} = \varepsilon \begin{pmatrix} m_1 \\ a_1 \\ v_1 \end{pmatrix} + \varepsilon^2 \begin{pmatrix} m_2 \\ a_2 \\ v_2 \end{pmatrix} + \varepsilon^3 \begin{pmatrix} m_3 \\ a_3 \\ v_3 \end{pmatrix} + o(\varepsilon^4), \tag{4.6}$$

$$N = \varepsilon^2 h_2 + \varepsilon^3 h_3 + o(\varepsilon^4), \tag{4.7}$$

$$\frac{\partial}{\partial t} = \frac{\partial}{\partial T_0} + \varepsilon \frac{\partial}{\partial T_1} + \varepsilon^2 \frac{\partial}{\partial T_2} + o(\varepsilon^3), \tag{4.8}$$

$$\frac{\partial A}{\partial t} = \frac{\partial A}{\partial T_1} + \varepsilon^2 \frac{\partial A}{\partial T_2} + o(\varepsilon^3), \tag{4.9}$$

where $T_0 = t$, $T_1 = \varepsilon t$, $T_2 = \varepsilon^2 t$. According to the the expressions (4.3) and (4.4), we get

$$\frac{\partial U}{\partial t} = (L_T + (\gamma_T - \gamma M)U + N = L_T U + (\gamma_T - \gamma)MU + N. \tag{4.10}$$

Taking (4.5)-(4.8) into (4.10) , we get

$$\frac{\partial}{\partial t} \left(\varepsilon \begin{pmatrix} m_1 \\ a_1 \\ v_1 \end{pmatrix} + \varepsilon^2 \begin{pmatrix} m_2 \\ a_2 \\ v_2 \end{pmatrix} + \varepsilon^3 \begin{pmatrix} m_3 \\ a_3 \\ v_3 \end{pmatrix} \right) = L_T \left(\varepsilon \begin{pmatrix} m_1 \\ a_1 \\ v_1 \end{pmatrix} + \varepsilon^2 \begin{pmatrix} m_2 \\ a_2 \\ v_2 \end{pmatrix} + \varepsilon^3 \begin{pmatrix} m_3 \\ a_3 \\ v_3 \end{pmatrix} \right)$$

$$+ (\varepsilon\gamma_1 + \varepsilon^2\gamma_2 + \varepsilon^3\gamma_3)M \times \left(\varepsilon \begin{pmatrix} m_1 \\ a_1 \\ v_1 \end{pmatrix} + \varepsilon^2 \begin{pmatrix} m_2 \\ a_2 \\ v_2 \end{pmatrix} + \varepsilon^3 \begin{pmatrix} m_3 \\ a_3 \\ v_3 \end{pmatrix} \right)$$

$$+ \varepsilon^2 h_2 + \varepsilon^3 h_3 + o(\varepsilon^4), \tag{4.11}$$

where

$$\frac{\partial}{\partial t}\left(\varepsilon\begin{pmatrix} m_1 \\ a_1 \\ v_1 \end{pmatrix} + \varepsilon^2 \begin{pmatrix} m_2 \\ a_2 \\ v_2 \end{pmatrix} + \varepsilon^3 \begin{pmatrix} m_3 \\ a_3 \\ v_3 \end{pmatrix}\right)$$

$$= \varepsilon^2 \frac{\partial}{\partial T_1}\begin{pmatrix} m_1 \\ a_1 \\ v_1 \end{pmatrix} + \varepsilon^3 \frac{\partial}{\partial T_1}\begin{pmatrix} m_2 \\ a_2 \\ v_2 \end{pmatrix} + \varepsilon^3 \frac{\partial}{\partial T_2}\begin{pmatrix} m_1 \\ a_1 \\ v_1 \end{pmatrix} + o(\varepsilon^4).$$

By comparing the coefficient of ε in (4.11), we get

$$L_T \begin{pmatrix} m_1 \\ a_1 \\ v_1 \end{pmatrix} = 0. \tag{4.12}$$

By comparing the coefficient of ε^2 in (4.11), we get

$$\frac{\partial}{\partial T_1}\begin{pmatrix} m_1 \\ a_1 \\ v_1 \end{pmatrix} = L_T \begin{pmatrix} m_2 \\ a_2 \\ v_2 \end{pmatrix} + \gamma_1 M \begin{pmatrix} m_1 \\ a_1 \\ v_1 \end{pmatrix} + h_2. \tag{4.13}$$

By comparing the coefficient of ε^3 in (4.11), we get

$$\frac{\partial}{\partial T_1}\begin{pmatrix} m_2 \\ a_2 \\ v_2 \end{pmatrix} + \frac{\partial}{\partial T_2} = L_T \begin{pmatrix} m_3 \\ a_3 \\ v_3 \end{pmatrix} + \gamma_1 M \begin{pmatrix} m_2 \\ a_2 \\ v_2 \end{pmatrix} + \gamma_2 M \begin{pmatrix} m_1 \\ a_1 \\ v_1 \end{pmatrix} + h_3. \tag{4.14}$$

Since L_T represents the linear operator of the system near the critical bifurcation point, $(m_1, a_1, v_1)^T$ is the linear combination of eigenvectors corresponding to eigenvalues of 0. For solving (4.12), we have

$$\begin{pmatrix} m_1 \\ a_1 \\ v_1 \end{pmatrix} = \begin{pmatrix} l_2 \\ l_3 \\ 1 \end{pmatrix}(W_1 \cdot e^{i\cdot k_1 \cdot \zeta} + W_2 \cdot e^{i\cdot k_2 \cdot \zeta} + W_3 \cdot e^{i\cdot k_3 \cdot \zeta}) + c.c., \tag{4.15}$$

where

$$l_2 = \frac{2f_3 b_{13}^*}{\mu_1(\delta + f_2) - 2f_3 b_{11}^*}, \quad l_3 = 1 + \frac{\mu_2(\delta - f_2)}{2f_2 \gamma_T}.$$

For the equation (4.13), we can get

$$
L_T \begin{pmatrix} m_2 \\ a_2 \\ v_2 \end{pmatrix} = \frac{\partial}{\partial T_1} \begin{pmatrix} m_1 \\ a_1 \\ v_1 \end{pmatrix} - \gamma_1 M \begin{pmatrix} m_1 \\ a_1 \\ v_1 \end{pmatrix} - h_2
$$

$$
= \frac{\partial}{\partial T_1} \begin{pmatrix} m_1 \\ a_1 \\ v_1 \end{pmatrix} - \gamma_1 \begin{pmatrix} c_{11}m_1 + c_{12}a_1 + c_{13}v_1 \\ c_{21}m_1 + c_{22}a_1 + c_{23}v_1 \\ c_{31}m_1 + c_{32}a_1 + c_{33}v_1 \end{pmatrix} - \begin{pmatrix} \frac{(1-\alpha r)^3}{(1-\alpha)^3} m_1^2 + r m_1 v_1 \\ -\frac{1}{\beta} m_1 v_1 \\ 0 \end{pmatrix}
$$

$$
= \begin{pmatrix} F_m \\ F_a \\ F_v \end{pmatrix}.
$$

$$(4.16)$$

According to the Fredholm solvability conditions, the vector to the right of equation (4.16) must be orthogonal to the zero eigenvector of L_T^+ (adjoint operator, also called conjugate operator), and there is a nontrivial solution to equation (4.16). We can calculate the zero eigenvector of L_T^+ is

$$
\begin{pmatrix} l_2' \\ 1 \\ l_3' \end{pmatrix} + c.c., (j = 1, 2, 3),
$$

where

$$
l_2' = \frac{2 f_3 b_{21}^*}{\mu_1 (\delta - f_2) - 2 f_3 b_{11}^*}, \quad l_3' = \frac{\delta - f_2 - 2\beta f_3 b_{22}^*}{2\beta f_3 \gamma_T}.
$$

Then, using the orthogonal string theorem

$$
(l_2', 1, l_3') \begin{pmatrix} F_m^i \\ F_a^i \\ F_v^i \end{pmatrix} = 0,
$$

$$(4.17)$$

where F_m^i, F_a^i, F_v^i represent the coefficients corresponding to $e^{ik_j \cdot \zeta}$ in F_m, F_a, F_v, which means

$$
\begin{pmatrix} F_m \\ F_a \\ F_v \end{pmatrix} = \begin{pmatrix} F_m^1 \\ F_a^1 \\ F_v^1 \end{pmatrix} e^{ik_1 \cdot \zeta} + \begin{pmatrix} F_m^2 \\ F_a^2 \\ F_v^2 \end{pmatrix} e^{ik_2 \cdot \zeta} + \begin{pmatrix} F_m^3 \\ F_a^3 \\ F_v^3 \end{pmatrix} e^{ik_3 \cdot \zeta}.
$$

According to (4.15) and (4.16), we get

$$
\begin{pmatrix} F_m^1 \\ F_a^1 \\ F_v^1 \end{pmatrix} = \begin{pmatrix} l_2 \frac{\partial W_1}{\partial T_1} \\ l_3 \frac{\partial W_1}{\partial T_1} \\ \frac{\partial W_1}{\partial T_1} \end{pmatrix} - \gamma_1 \begin{pmatrix} l_2 c_{11} W_1 + l_3 c_{12} W_1 + c_{13} W_1 \\ l_2 c_{21} W_1 + l_3 c_{22} W_1 + c_{23} W_1 \\ l_2 c_{31} W_1 + l_3 c_{32} W_1 + c_{33} W_1 \end{pmatrix} - \begin{pmatrix} 2\frac{(1-\alpha r)^3}{(1-\alpha)^3} l_2^2 + 2rl_2 \\ -\frac{1}{\beta} l_2 \\ 0 \end{pmatrix} \overline{W}_2 \overline{W}_3,
$$
$$(4.18)$$

$$
\begin{pmatrix} F_m^2 \\ F_a^2 \\ F_v^2 \end{pmatrix} = \begin{pmatrix} l_2 \frac{\partial W_2}{\partial T_1} \\ l_3 \frac{\partial W_2}{\partial T_1} \\ \frac{\partial W_2}{\partial T_1} \end{pmatrix} - \gamma_1 \begin{pmatrix} l_2 c_{11} W_2 + l_3 c_{12} W_2 + c_{13} W_2 \\ l_2 c_{21} W_2 + l_3 c_{22} W_2 + c_{23} W_2 \\ l_2 c_{31} W_2 + l_3 c_{32} W_2 + c_{33} W_2 \end{pmatrix} - \begin{pmatrix} 2\frac{(1-\alpha r)^3}{(1-\alpha)^3} l_2^2 + 2rl_2 \\ -\frac{1}{\beta} l_2 \\ 0 \end{pmatrix} \overline{W}_1 \overline{W}_3,
$$
$$(4.19)$$

$$
\begin{pmatrix} F_m^3 \\ F_a^3 \\ F_v^3 \end{pmatrix} = \begin{pmatrix} l_2 \frac{\partial W_3}{\partial T_1} \\ l_3 \frac{\partial W_3}{\partial T_1} \\ \frac{\partial W_3}{\partial T_1} \end{pmatrix} - \gamma_1 \begin{pmatrix} l_2 c_{11} W_3 + l_3 c_{12} W_3 + c_{13} W_3 \\ l_2 c_{21} W_3 + l_3 c_{22} W_3 + c_{23} W_3 \\ l_2 c_{31} W_3 + l_3 c_{32} W_3 + c_{33} W_3 \end{pmatrix} - \begin{pmatrix} 2\frac{(1-\alpha r)^3}{(1-\alpha)^3} l_2^2 + 2rl_2 \\ -\frac{1}{\beta} l_2 \\ 0 \end{pmatrix} \overline{W}_1 \overline{W}_2.
$$
$$(4.20)$$

Substituting (4.18)-(4.20) into (4.17), we get

$$
(l_2 l_2' + l_3 + l_3') \frac{\partial W_1}{\partial T_1} = \gamma_1 [l_2'(l_2 c_{11} + l_3 c_{12} + c_{13}) + l_2 c_{21} + l_3 c_{22} + c_{23} + l_3'(l_2 c_{31}
$$
$$
+ l_3 c_{32} + c_{33})] W_1 + [2\frac{(1 - \alpha r)^3}{(1 - \alpha)^3} l_2 l_2' + 2rl_2 l_2' - 2\frac{1}{\beta} l_2] \overline{W}_2 \overline{W}_3,
$$

$$
(l_2 l_2' + l_3 + l_3') \frac{\partial W_2}{\partial T_1} = \gamma_1 [l_2'(l_2 c_{11} + l_3 c_{12} + c_{13}) + l_2 c_{21} + l_3 c_{22} + c_{23} + l_3'(l_2 c_{31}
$$
$$
+ l_3 c_{32} + c_{33})] W_2 + [2\frac{(1 - \alpha r)^3}{(1 - \alpha)^3} l_2 l_2' + 2rl_2 l_2' - 2\frac{1}{\beta} l_2] \overline{W}_1 \overline{W}_3,
$$

$$
(l_2 l_2' + l_3 + l_3') \frac{\partial W_3}{\partial T_1} = \gamma_1 [l_2'(l_2 c_{11} + l_3 c_{12} + c_{13}) + l_2 c_{21} + l_3 c_{22} + c_{23} + l_3'(l_2 c_{31}
$$
$$
+ l_3 c_{32} + c_{33})] W_3 + [2\frac{(1 - \alpha r)^3}{(1 - \alpha)^3} l_2 l_2' + 2rl_2 l_2' - 2\frac{1}{\beta} l_2] \overline{W}_1 \overline{W}_2.
$$
$$(4.21)$$

Then, substituting the equation (4.15) into (4.16), we calculate

$$
\begin{pmatrix} m_2 \\ a_2 \\ v_2 \end{pmatrix} = \begin{pmatrix} M_0 \\ A_0 \\ V_0 \end{pmatrix} + \sum_{i=1}^{3} \begin{pmatrix} M_i \\ A_i \\ V_i \end{pmatrix} e^{ik_i \cdot \zeta} + \sum_{i=1}^{3} \begin{pmatrix} M_{ii} \\ A_{ii} \\ V_{ii} \end{pmatrix} e^{i2k_i \cdot \zeta} + \begin{pmatrix} M_{12} \\ A_{12} \\ V_{12} \end{pmatrix} e^{i(k_1 - k_2) \cdot \zeta}
$$
$$
+ \begin{pmatrix} M_{23} \\ A_{23} \\ V_{23} \end{pmatrix} e^{i(k_2 - k_3) \cdot \zeta} + \begin{pmatrix} M_{31} \\ A_{31} \\ V_{31} \end{pmatrix} e^{i(k_3 - k_1) \cdot \zeta} + c.c.
$$
$$(4.22)$$

The coefficients in equation (4.22) are obtained by solving the linear equation

corresponding to ε^0, $\varepsilon^{i2k_i\cdot\varsigma}$, $e^{ik_i\cdot\varsigma}$, $e^{i(k_j-k_m)\cdot\varsigma}$. Therefore, we obtain

$$\begin{pmatrix} M_0 \\ A_0 \\ V_0 \end{pmatrix} = \begin{pmatrix} m_0 \\ a_0 \\ v_0 \end{pmatrix}(|W_1|^2 + |W_2|^2 + |W_3|^2),$$

$$M_i = l_2 V_i, A_i = l_3 V_i, \qquad \begin{pmatrix} M_{ii} \\ A_{ii} \\ V_{ii} \end{pmatrix} = \begin{pmatrix} m_{11} \\ a_{11} \\ v_{11} \end{pmatrix}W_i^2, \qquad \begin{pmatrix} M_{ij} \\ A_{ij} \\ V_{ij} \end{pmatrix} = \begin{pmatrix} m_{ij} \\ a_{ij} \\ v_{ij} \end{pmatrix}W_i\overline{W}_j.$$

For the equation (4.14), we get

$$L_T \begin{pmatrix} m_3 \\ a_3 \\ v_3 \end{pmatrix} = -\gamma_2 M \begin{pmatrix} c_{11}m_1 + c_{12}a_1 + c_{13}v_1 \\ c_{21}m_1 + c_{22}a_1 + c_{23}v_1 \\ c_{31}m_1 + c_{32}a_1 + c_{33}v_1 \end{pmatrix} - \gamma_1 M \begin{pmatrix} c_{11}m_2 + c_{12}a_2 + c_{13}v_2 \\ c_{21}m_2 + c_{22}a_2 + c_{23}v_2 \\ c_{31}m_2 + c_{32}a_2 + c_{33}v_2 \end{pmatrix}$$

$$+ \frac{\partial}{\partial T_1} \begin{pmatrix} m_2 \\ a_2 \\ v_2 \end{pmatrix} - \begin{pmatrix} 2\frac{(1-\alpha r)^3}{(1-\alpha)^3}m_1 m_2 + rm_1 v_2 + m_2 v_1 - \frac{(1-\alpha r)^4}{(1-\alpha)^4}m_1^3 \\ -\frac{1}{\beta}(m_1 v_2 + m_2 v_1) \\ 0 \end{pmatrix}$$

$$+ \frac{\partial}{\partial T_2} \begin{pmatrix} m_1 \\ a_1 \\ v_1 \end{pmatrix} = \begin{pmatrix} H_m \\ H_a \\ H_v \end{pmatrix}.$$

$$(4.23)$$

Similar to the above analysis, we take $e^{ik_1\cdot\varsigma}$, $e^{ik_2\cdot\varsigma}$, $e^{ik_3\cdot\varsigma}$ of H_m and H_a, H_v in system (4.23), and we get

$$\begin{pmatrix} H_m^1 \\ H_a^1 \\ H_v^1 \end{pmatrix} = \begin{pmatrix} l_2\frac{\partial V_1}{\partial T_1} \\ l_3\frac{\partial V_1}{\partial T_1} \\ \frac{\partial V_1}{\partial T_1} \end{pmatrix} + \begin{pmatrix} l_2\frac{\partial W_1}{\partial T_2} \\ l_3\frac{\partial W_1}{\partial T_2} \\ \frac{\partial W_1}{\partial T_2} \end{pmatrix} - \gamma_1 \begin{pmatrix} l_2 C_{11} + l_3 C_{12} + C_{13} \\ l_2 C_{21} + l_3 C_{22} + C_{23} \\ l_2 C_{31} + l_3 C_{32} + C_{33} \end{pmatrix}V_1$$

$$- \gamma_2 \begin{pmatrix} l_2 C_{11} + l_3 C_{12} + C_{13} \\ l_2 C_{21} + l_3 C_{22} + C_{23} \\ l_2 C_{31} + l_3 C_{32} + C_{33} \end{pmatrix}W_1 + \begin{pmatrix} G_{11}|W_1|^2 + G_{12}(|W_2|^2 + |W_3|^2) \\ G_{21}|W_1|^2 + G_{22}(|W_2|^2 + |W_3|^2) \\ 0 \end{pmatrix}W_1$$

$$- \begin{pmatrix} 2\frac{(1-\alpha r)^3}{(1-\alpha)^3}l_2^2 + 2rl_2 \\ -2\frac{1}{\beta}l_2 \\ 0 \end{pmatrix}\overline{W}_2\overline{V}_3 - \begin{pmatrix} 2\frac{(1-\alpha r)^3}{(1-\alpha)^3}l_2^2 + 2rl_2 \\ -2\frac{1}{\beta}l_2 \\ 0 \end{pmatrix}\overline{W}_3\overline{V}_2.$$

$$(4.24)$$

The remaining two equations can be obtained by changing the subscript of W, and $G_{11} = \frac{2(1-\alpha r)^3}{(1-\alpha)^3}l_2 m_0 + \frac{2(1-\alpha r)^3}{(1-\alpha)^3}l_2 m_{11} + rl_2 v_0 + rl_2 v_{11} + m_0 + m_{11} - \frac{(1-\alpha r)^4}{(1-\alpha)^4}l_2^2$,

$G_{12} = \frac{2(1-\alpha r)^3}{(1-\alpha)^3} l_2 m_0 + \frac{2(1-\alpha r)^3}{(1-\alpha)^3} l_2 m_{12} + r l_2 v_0 + r l_2 v_{12} + m_0 + m_{11} - \frac{(1-\alpha r)^4}{(1-\alpha)^4} l_2^2$,

$G_{21} = \frac{1}{\beta}(l_2 v_0 + l_2 v_{11} + m_0 + m_{11})$,

$G_{22} = \frac{1}{\beta}(l_2 v_0 + l_2 v_{12} + m_0 + m_{12})$.

Similar to the second section, by using the Fredholm solvability conditions for (4.24), we get equations as follows:

$$(l_2 l_2' + l_3 + l_3')(\frac{\partial V_1}{\partial T_1} + \frac{\partial W_1}{\partial T_2})$$

$$= (\gamma_1 V_1 + \gamma_2 W_1)[l_2'(l_2 c_{11} + l_3 c_{12} + c_{13}) + (l_2 c_{21} + l_3 c_{22} + c_{23}) + l_3'(l_2 c_{31} + l_3 c_{32}$$

$$+ c_{33})] - l_2'[G_{11}|W_1|^2 + G_{12}(|W_2|^2 + |W_3|^2)]W_1 - [G_{21}|W_1|^2 + G_{22}(|W_2|^2$$

$$+ |W_3|^2)]W_1 + [2\frac{(1-\alpha r)^3}{(1-\alpha)^3} l_2^2 + 2 r l_2 - 2\frac{1}{\beta} l_2)](\overline{W}_2 \overline{V}_3 + \overline{W}_3 \overline{V}_2).$$

$$(4.25)$$

The remaining two equations can be obtained by changing the subscripts of W and V.

Let $A_i = l_3 A_i^m = l_2 A_i^a = l_2 l_3 A_i^v$ be the coefficient of $e^{ik_i \cdot \zeta}$ (i=1,2,3), and then we get

$$\begin{pmatrix} A_i^m \\ A_i^a \\ A_i^v \end{pmatrix} = \varepsilon \begin{pmatrix} l_2 \\ l_3 \\ 1 \end{pmatrix} W_i + \varepsilon^2 \begin{pmatrix} l_2 \\ l_3 \\ 1 \end{pmatrix} V_i + o(\varepsilon^3), (i = 1, 2, 3). \qquad (4.26)$$

According to the (4.21) and (4.25), and using (4.9), (4.26) to merge the variables, we can obtain the corresponding coefficients in equation (4.1):

$$\begin{cases} B = l_2'(l_2 c_{11} + l_3 c_{12} + c_{13}) + (l_2 c_{21} + l_3 c_{22} + c_{23}) + l_3'(l_2 c_{31} + l_3 c_{32} + c_{33}), \\[1.5ex] \tau_0 = -\dfrac{l_2 l_2' + l_3 + l_3'}{\gamma_T B}, \\[2ex] h = \dfrac{-2 l_2' 2 \frac{(1-\alpha r)^3}{(1-\alpha)^3} l_2^2 + 2 r l_2 + 2 \frac{1}{\beta} l_2}{\gamma_T B}, \\[2ex] g_1 = -\dfrac{l_2' G_{11} + G_{21}}{\gamma_T B}, \\[2ex] g_2 = -\dfrac{l_2' G_{12} + G_{22}}{\gamma_T B}, \\[2ex] \nu = -\dfrac{\gamma_T - \gamma}{\gamma_T}. \end{cases}$$

$$(4.27)$$

5. Main results

5.1. Pattern selection

The amplitude equation has same form for different systems, but the difference is that the coefficients of each term are different. Next, we use the amplitude equation to analyze the dynamical system near the unstable point. A stable Turing pattern

corresponds to the steady-state solution of the system (4.1), and each amplitude in (4.1) can be decomposed into a phase angle φ_j and a mode $\rho_j = |A_j|$. Then, by substituting (4.1) with $A_j = \rho_j exp(j\varphi_j)$ and separating the real and imaginary parts, we can get four real variable equations in the following form:

$$
\begin{cases}
\tau_0 \dfrac{\partial \varphi}{\partial t} = -h \dfrac{\rho_1^2 \rho_2^2 + \rho_1^2 \rho_3^2 + \rho_2^2 \rho_3^2}{\rho_1 \rho_2 \rho_3} sin\varphi, \\
\tau_0 \dfrac{\partial \rho_1}{\partial t} = \nu\rho_1 + h\rho_2\rho_3 cos\varphi - g_1\rho_1^3 - g_2(\rho_2^2 + \rho_3^2)\rho_1, \\
\tau_0 \dfrac{\partial \rho_2}{\partial t} = \nu\rho_2 + h\rho_1\rho_3 cos\varphi - g_1\rho_2^3 - g_2(\rho_1^2 + \rho_3^2)\rho_1, \\
\tau_0 \dfrac{\partial \rho_3}{\partial t} = \nu\rho_3 + h\rho_1\rho_2 cos\varphi - g_1\rho_3^3 - g_2(\rho_1^2 + \rho_2^2)\rho_1,
\end{cases}
\tag{5.1}
$$

where $\varphi = \varphi_1 + \varphi_2 + \varphi_3$. The system (5.1) has five pattern types and the stability range, which can be obtained by calculation:

(i) The stationary state: $\rho_1 = \rho_2 = \rho_3 = 0$, and when $\nu < \nu_2 = 0$, the stationary state is stable.

(ii) The stripe pattern: $\rho_1 = \sqrt{\frac{\nu}{g_1}}$, and $\rho_2 = \rho_3 = 0$, which exist when $\nu > 0$. When the stable range is $\nu > \nu_3 = \frac{h^2 g_1}{(g_2 - g_1)^2}$, the unstable range is $\nu > \nu_3$.

(iii) Two spots pattern: $\rho_+ = \frac{|h| + \sqrt{h^2 + 4\nu(g_1 + 2g_2)}}{2(g_1 + 2g_2)}$, $\rho_- = \frac{|h| - \sqrt{h^2 + 4\nu(g_1 + 2g_2)}}{2(g_1 + 2g_2)}$, which exist when $\nu > \nu_1 = \frac{-h^2}{4(g_1 + 2g_2)}$. For the ρ_+, the stable range is $\nu < \nu_4 = \frac{2g_1 + g_2}{(g_2 - g_1)^2}h^2$ and ρ_- is always unstable.

(iv) The mixed state: $\rho_1 = \frac{|h|}{g_2 - g_1}$, $\rho_2 = \rho_3 = \sqrt{\frac{\nu - g_1\rho_1^2}{g_1 + g_2}}$, which exist when $\nu > \nu_3$, and the pattern always is unstable.
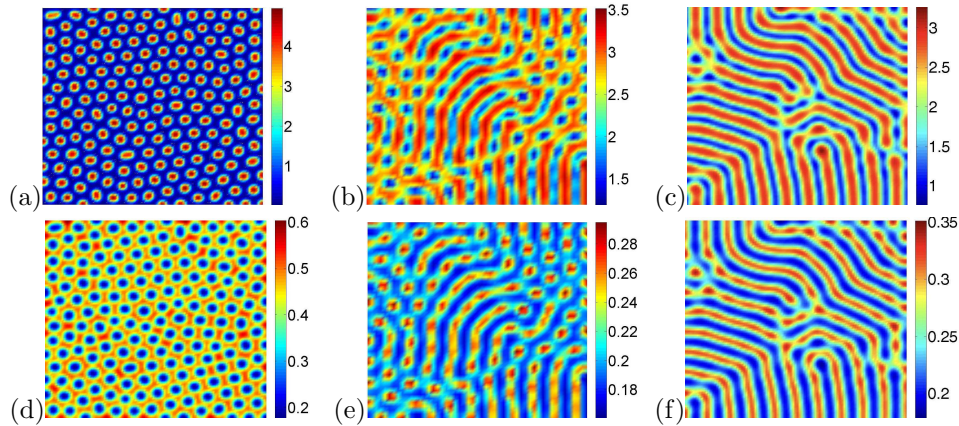
Figure 5.   Corresponding mussel spatial distribution reaches steady state with the change of μ_1. (a) $\mu_1 = 0.005$; (b) $\mu_1 = 0.015$; (c) $\mu_1 = 0.025$; (d) $\mu_1 = 0.035$; (e) $\mu_1 = 0.045$; (f) $\mu_1 = 0.05$. For the other parameters, we choose $\mu_2 = 0.05, \beta = \frac{2}{15}, r = 1.32, \alpha = \frac{2}{3}, \gamma = 0.45$.

Table 1. Simulation parameters in Figure 5

Order	μ_1	μ_2	α	β	r	γ	h	ν	Scope of ν
1	0.025	0.05	$\frac{2}{3}$	$\frac{2}{15}$	1.39	0.5	-10.047329821	0.39504331002	(ν_2, ν_3)
2	0.05	0.05	$\frac{2}{3}$	$\frac{2}{15}$	1.35	0.167	-0.41790322403	0.07283500764	(ν_3, ν_4)
3	0.04	0.05	$\frac{2}{3}$	$\frac{2}{15}$	1.32	0.286	-0.88340742031	0.04807945028	$(\nu_4, +\infty)$

5.2. Within a certain range, the higher the γ, the smaller the average density of mussels

Next, we carry out numerical simulation for the spatiotemporal dynamic analysis of the system (2.3). By analyzing the dynamics of the system and searching the literatures, we obtain the conditions to occur the Turing instability and the values of each parameters. After the parameters are determined, we simulate the spatial distribution pattern of the mussel in the system (2.3), and study the influence of the value of the parameter on the spatial pattern of mussels. In order to better display the simulation effect, the forward difference scheme is adopted based on Neumann boundary condition. Parameters such as time interval and step size are selected as follows: the space area is $[0, 50]$, the time interval of T is $[0, 5000]$, the space step is $\triangle h = 1$ and the time step is $\triangle t = 0.005$. The initial value is the random perturbation value of the coexistence equilibrium point E^*. With the setting of the above parameters, we get the following results.

Figure 6 describes the evolution process of the spatial pattern of mussels over time. In this process, the mussel gradually aggregates into a connected strip distribution (see Figure 6(b)) from the initial irregular scattered distribution (see Figure 6(a)). Then, it continues to evolve into a mixed distribution of square and short strips (see Figure 6(c)), and finally forms a mixed distribution of short strips with a small number of clusters (see Figure 6(d)), when it reaches the steady state.
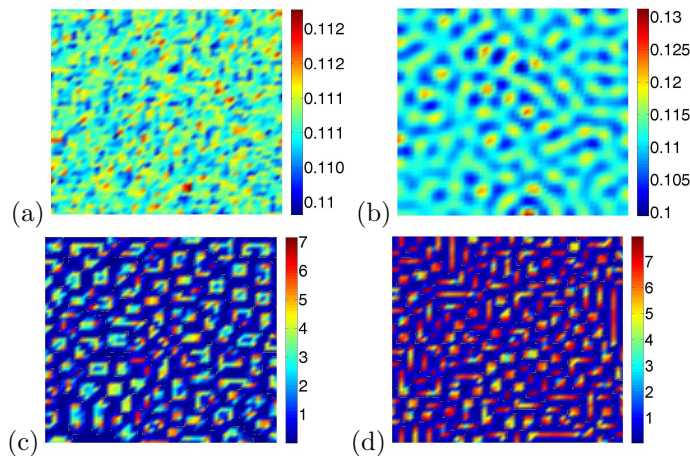
Figure 6. Describe the evolution of mussel spatial pattern over time. (a) $t = 10$; (b) $t = 300$; (c) $t = 650$; (d) $t = 5000$. For the other parameters, we choose $\mu_1 = 0.025, \mu_2 = 0.05, \beta = \frac{2}{15}, \alpha = \frac{2}{3}, \gamma = 0.45, r = 1.05$.

Figure 7 depicts the relationship between the spatial mean density of mussels and parameter γ. Combined with the actual biological significance, γ represents the spatial distance parameter between mussel and algae. From Figure 7, we find

that with the increase of spatial distance γ, and the average density change rate of mussel gradually approaches 0, because the nonlocal item has influence on pattern formation of mussels within a certain range. When spatial distance parameter continues to increase, nonlocal effects between mussels and algaes will become very small. at this time, other parameters, such as mussel diffusion rate and predation rate, affect the spatial pattern of mussels.
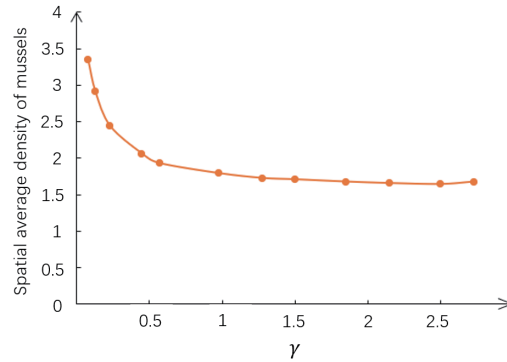
Figure 7. The density of mussels at steady state change with the parameter γ. For other parameters, we select $\alpha = \frac{2}{3}$, $\beta = \frac{2}{15}$ and $r = 1.05$, $\mu_1 = 0.025$, $\mu_2 = 0.05$.

5.3. The r and μ_1 respectively affect the pattern type and average density of mussels

We take the parameter γ between $(0, 0.5)$. When the nonlocal effect on mussels is obvious, the influence of other parameters on the pattern of mussels is analyzed.
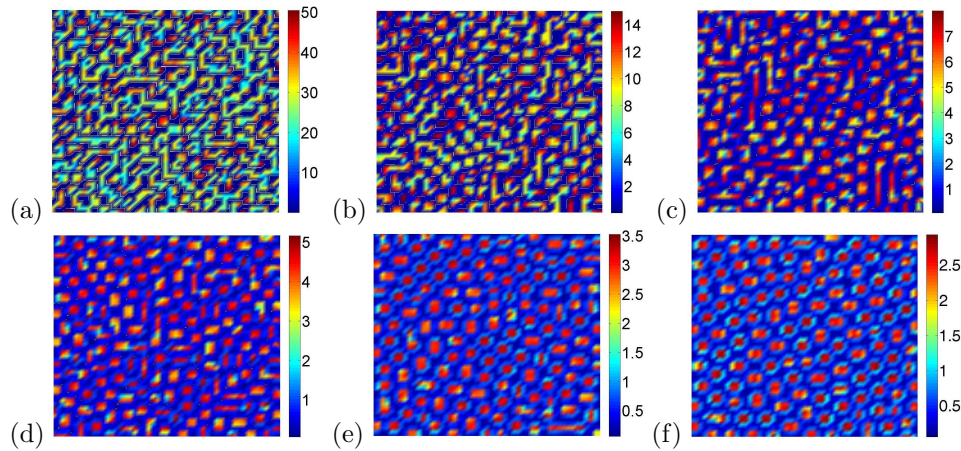
Figure 8. Corresponding mussel spatial distribution reaches steady state with the change of μ_1. (a) $\mu_1 = 0.005$; (b) $\mu_1 = 0.015$; (c) $\mu_1 = 0.025$; (d) $\mu_1 = 0.035$; (e) $\mu_1 = 0.045$; (f) $\mu_1 = 0.05$. For the other parameters, we choose $\mu_2 = 0.05, \beta = \frac{2}{15}, r = 1.1, \alpha = \frac{2}{3} and \gamma = 0.45$.

Firstly, the influence of parameter μ_1, which represents the diffusion rate of mussels in the actual biological sense, and on the formation of mussel bed was

simulated. Figure 8 describes the spatial structural change of mussels when reaching steady state with the change of the mussel's diffusion rate while other parameters are quantified. As is seen from Figure 8(a) to Figure 8(f), with the increase of μ_1, the "maze" spatial pattern of mussels which composed of irregular and dense strips gradually forms short strips and square "new mixed" pattern, and finally forms regular square pattern. An interesting phenomenon here is the emergence of a new type of "square" pattern in addition to strip, spot and mixed patterns. For "square" pattern, they are similar to regular spot pattern on a small scale, but because of the increased diffusivity, intraspecific competition is reduced, thus forming a more stable square pattern. In large scale, the "square" distribution is closely related to the "strip" distribution. Due to rapid diffusion, intraspecies competition and intraspecies dependence were weakened and a discontinuous square pattern was formed. Considering that there haven't square pattern been found in previous studies, we infer that the nonlocal interaction between mussels and algaes leads to the generation of "square" pattern in the mussel beds.

In addition, it is worth mentioning that when the diffusion rate of mussels is very high. If the nonlocal interaction is not taken into account, the predation of mussels will be limited by space. Due to the influence of the nonlocal interaction, the mussels can keep still predation and survive in space, which will not become extinct.
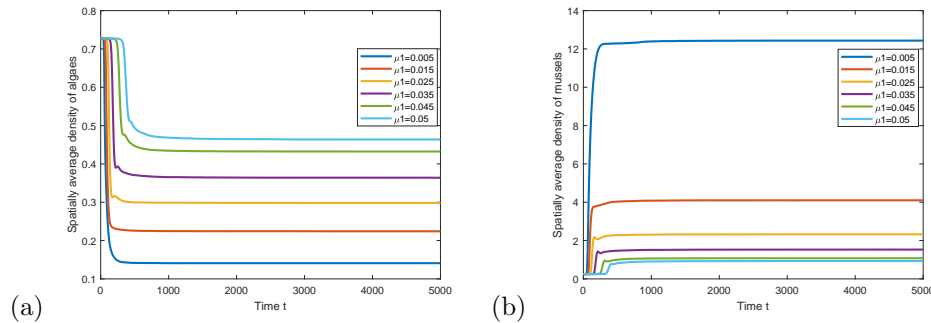
Figure 9. Depict the evolution of the spatial mean density of the corresponding algaes and mussels over time when different values of μ_1 are taken. For the other parameters, we chose: $\mu_2 = 0.05, \beta = \frac{2}{15}, r = 1.1, \alpha = \frac{2}{3}, \gamma = 0.45$.

Figure 9 describes the change of the spatial mean density of algaes and mussels with time when μ_1 is different. It can be seen from these two figures that the average density of mussels decreases when they reach steady state, while the density of algae increases with the increase of μ_1, which is consistent with the normal density inhibition relationship between predation and prey. The reason for the decrease of mussel density may be related to the structural characteristics of mussel itself. Mussels depend on byssus for feeding and locomotion, when the diffusion rate of mussels is lower, the mussel is essentially fixed to the sediment, which causes byssus to be able to feed more fully. However, when the diffusion rate is higher, there is less byssus available for feeding, which leads to the decrease of mussel density.

Next, we simulate the influence of parameter μ_1 change on the spatial distribution structure of mussels when $r = 1.32$. As is seen from Figure 10(a) to Figure 10(f), the spatial distribution of mussels gradually evolves from the initial irregular
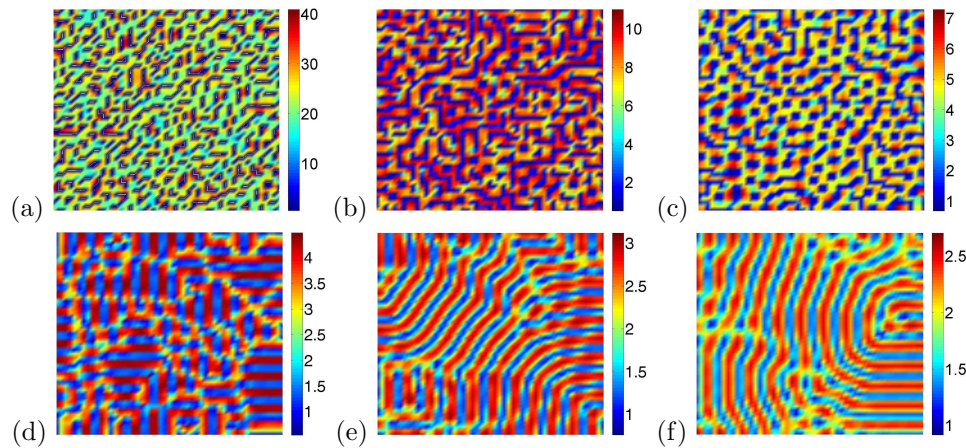
Figure 10.   Corresponding mussel spatial distribution reaches steady state with the change of μ_1. (a) $\mu_1 = 0.005$; (b) $\mu_1 = 0.015$; (c) $\mu_1 = 0.025$; (d) $\mu_1 = 0.035$; (e) $\mu_1 = 0.045$; (f) $\mu_1 = 0.05$. For the other parameters, we chose: $\mu_2 = 0.05, \beta = \frac{2}{15}, r = 1.32, \alpha = \frac{2}{3}, \gamma = 0.45$.

"maze" pattern to the "flower clusters" pattern (see Figure 10(c)) and eventually evolves into the regular "strip" pattern (see Figure 10(d), Figure 10(e) and Figure 10(f)). Parameter r can be understood as the predation rate of mussels to algaes. With the increase of predation rate, intraspecies competition and intraspecies dependence are enhanced, which leads to form a "strip" structure. By longitudinal comparison with Figure 8, it can be found that predation rate is the main factor that affects the pattern structure of mussels when r is different. That is because although μ_1 is also changing, the change of r leads to the change of pattern type.

In Figure 11, we still study the variation of the spatial average density of algaes and mussels corresponding to different parameters μ_1 over time. Considering the high density of mussels at $\mu_1 = 0.005$, the isolation mapping and analysis are therefore carried out. On the whole, the changing trend of the average density of algaes and mussels is consistent with Figure 9, Figure 11(a) and Figure 11(b), showing that the mussel have a better living environment due to its small diffusion rate and high predation rate. Although the predation rate of mussels increases, the larger diffusion rate still results in a decrease in mussel density.

Figure 12 analyzes the effect of predation rate r on the spatial distribution structure of mussels. With the change of r, in addition to "new mixed" pattern and "flower clusters" pattern, "hole" distribution pattern also appeared, as shown in Figure 12(e). It can be seen that with the increase of predation rate, the mussel aggregation degree gradually form from small clusters to short strips, then to long strips, and finally to a larger "hole" aggregation degree. The intraspecies competition increase with the increase of predation rate, mussels gradually form strip and band structures. As the predation rate continues to increase, due to the inhibitory relationship between mussels and algaes, the band structure of mussels is destroyed, and the uniform hole distribution is formed under the nonlocal interaction. It can be seen that the change of parameter r has a great influence on the formation of different pattern types of mussels in space. In addition, the nonlocal interaction ensures the survival of mussels when the predation resources are limited.

From the above analysis, it can be seen that under the nonlocal interaction, the
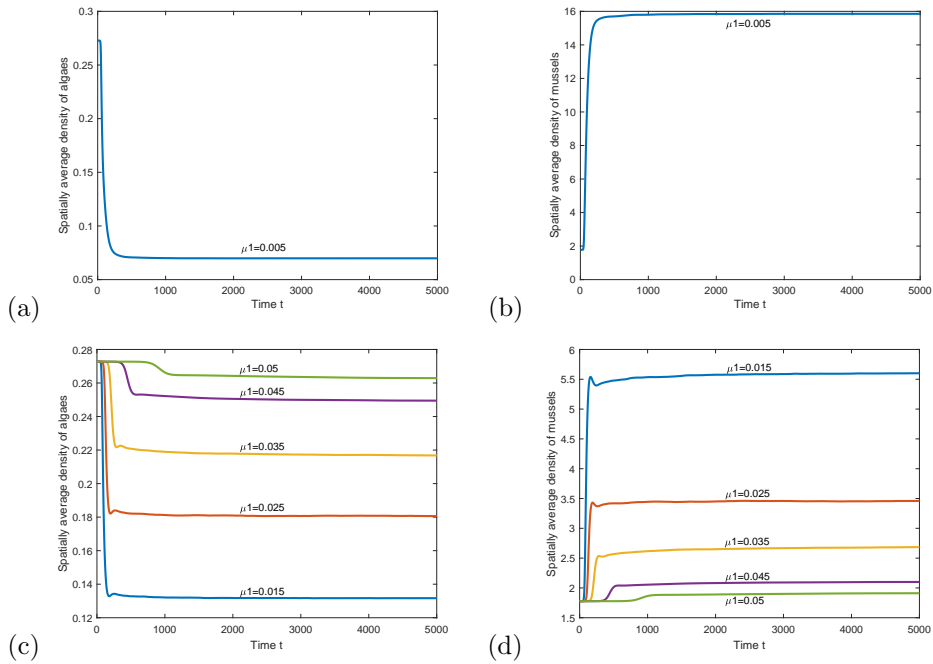
Figure 11. Depict the evolution of the spatial mean density of the corresponding algaes and mussels over time when different values of μ_1 are taken. For the other parameters, we cho0se: $\mu_2 = 0.05, \beta = \frac{2}{15}, r = 1.32, \alpha = \frac{2}{3}$ and $\gamma = 0.45$.

predation rate of mussels has a great influence on the type of spatial pattern, while the diffusion rate mainly affects the average density of mussels.

6. Conclusions

As an important habitat and food source of coastal ecosystem, the study of mussel beds is of key significance. Many studies have simulated and analyzed the formation mechanism and spatial structure of mussel beds, and obtained important theoretical results, but these studies only consider the local effect, while in fact, mussels can prey on algae at all locations in space, not just the current location and the current time. Based on the model proposed by Van de Koppel et al., this paper introduces the nonlocal interaction between mussels and algaes into the system, which hope to study the spatial structure of the population from the internal relationship between the populations. Through the dynamic analysis and simulation of the new system, it is found that the nonlocal interaction can induce the generation of self-organizing mussel beds. The effects of parameters on the spatial distribution of mussels are studied under nonlocal interaction. The results show that the diffusion rate and the predation rate of mussels have a great influence on the new pattern structure of mussels. In addition, we also study the effects of nonlocal interaction parameters γ on the spatial structure of mussels, and find that nonlocal interaction plays an important role in the sustainable survival of mussels, which will help to study the stability of mussel beds.
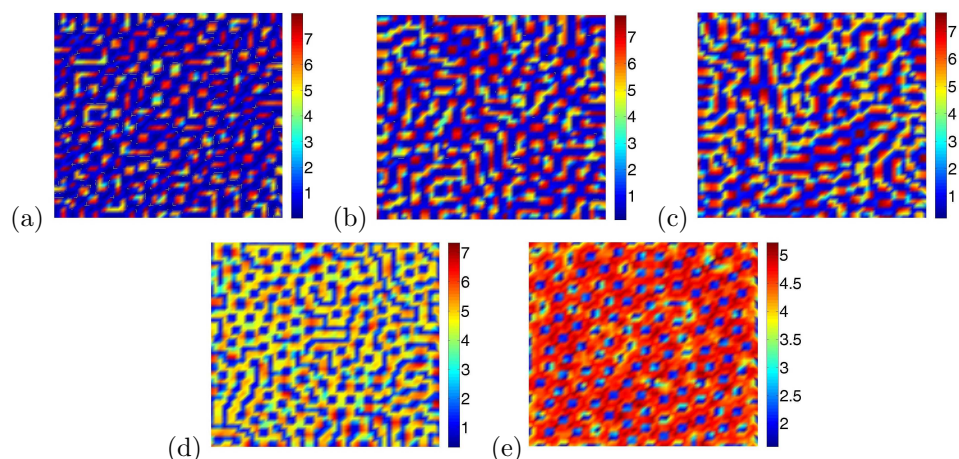
Figure 12. Corresponding mussel spatial distribution reaches steady state with the change of r. (a) $r = 1.05$; (b) $r = 1.19$; (c) $r = 1.25$; (d) $r = 1.32$; (e) $r = 1.39$; (f) $r = 0.05$. For the other parameters, we chose: $\mu_2 = 0.05, \beta = \frac{2}{15}, \mu_1 = 0.025, \alpha = \frac{2}{3}, \gamma = 0.45$.

Based on the original system, this paper introduces a new action term and combines the data for simulation analysis, we conclude that nonlocal interaction is another mechanism for the spatial pattern of mussel beds. Compared with previous studies, we find more pattern types, such as "square" pattern and "hole" pattern, which will be helpful to study the ecological functions corresponding to the pattern. However, we don't take climate into account in this paper, and in fact, given the high temperatures that mussel beds are now experiencing, climate is one of the factors that needs to be taken into account. In addition, we haven't analyzed and studied the ecological function corresponding to the patterns for the time being. In the future work, I hope to continue my research on mussel beds, and combine the above problems with the model and practice to conduct more research so as to make my research more meaningful and connected with the reality.

References

[1] M. J. Anderson, *Animal-sediment relationships re-visited: Characterising species' distributions along an environmental gradient using canonical analysis and quantile regression splines*, Journal of Experimental Marine Biology and Ecology, 2008, 366, 16–27.

[2] N. F. Britton, *Spatial Structures and Periodic Travelling Waves in an Integro-Differential Reaction-Diffusion Population Model*, SIAM Journal on Applied Mathematics, 1990, 50, 1663–1688.

[3] R. A. Cangelosi, D. Wollkind, B. J. Kealy-Dichone and I. Chaiya, *Nonlinear stability analyses of Turing patterns for a mussel-algae model*, Journal of Mathematical Biology, 2015, 70, 1249–1294.

[4] S. Chen and J. Yu, *Dynamics of a diffusive predatorCprey system with a nonlinear growth rate for the predator*, Journal of Differential Equations, 2016, 260, 7923–7939.

[5] S. Chen and J. Yu, *Stability and bifurcation on predator-prey systems with*

nonlocal prey competition, Discrete & Continuous Dynamical Systems, 2018, 38, 43–62.

[6] S. R. Choudhury, *Turing Instability in Competition Models with Delay I: Linear Theory*, SIAM Journal on Applied Mathematics, 1994, 54, 1425–1450.

[7] T. Faria, *Normal forms and Hopf bifurcation for partial differential equations with delays*, Transactions of the American Mathematical Society, 2000, 352, 2217–2238.

[8] M. Frechette and E. Bourget, *Food-Limited Growth of Mytilus edulis L. in Relation to the Benthic Boundary Layer*, Canadian Journal of Fisheries and Aquatic Sciences, 1985, 42, 1166–1170.

[9] S. Gan and Z. Yu, *The approach of solutions for the nonlocal diffusion equation to traveling fronts*, Journal of Nonlinear Modeling and Analysis, 2020, 2(2), 205–226.

[10] S. A. Gourley, A. Liu and J. Wu, *Some Vector Borne Diseases with Structured Host Populations: Extinction and Spatial Spread*, SIAM Journal on Applied Mathematics, 2007, 67, 408–433.

[11] S. A. Gourley and S. Ruan, *Convergence and Travelling Fronts in Functional Differential Equations with Nonlocal Terms: A Competition Model*, SIAM Journal on Mathematical Analysis, 2003, 35, 806–822.

[12] F. Guichard, P. M. Halpin, G. W. Allison, J. Lubchenco and B. A. Menge, *Mussel Disturbance Dynamics: Signatures of Oceanographic Forcing from Local Interactions*, The American Naturalist, 2003, 161, 889–904.

[13] Z. Guo, G. Sun, Z. Wang, Z. Jin, L. li and C. Li, *Spatial dynamics of an epidemic model with nonlocal infection*, Applied Mathematics and Computation, 2020, 377, Article ID 125158.

[14] W. S. C. Gurney and A. R. Veitch, *Self-organization, scale and stability in a spatial predator-prey interaction*, Bulletin of Mathematical Biology, 2000, 62, 61–86.

[15] F. Hamel and L. Ryzhik, *On the nonlocal FisherCKPP equation: Steady states, spreading speed and global bounds*, Nonlinearity, 2014, 27, 2735–2753.

[16] B. Han and Z. Wang, *Turing Patterns of a Lotka-Volterra Competitive System with Nonlocal Delay*, International Journal of Bifurcation and Chaos, 2018, 28, Artcile ID 1830021.

[17] B. Han and Y. Yang, *On a predator-prey reaction-diffusion model with nonlocal effects*, Communications in Nonlinear Science and Numerical Simulation, 2017, 46, 49–61.

[18] J. V. Hardenberg, E. Meron, M. Shachak and Y. Zarmi, *Diversity of Vegetation Patterns and Desertification*, Physval Review Letters, 2001, 87, Article ID 198101.

[19] M. P. Hassell, H. N. Comins and R. M. May, *Species coexistence and self-organizing spatial dynamics*, Natura, 1994, 370, 290–292.

[20] C. G. Jones, J. H. Lawton and M. Shachak, *Positive and Negative Effects of Organisms as Physical Ecosystem Engineers*, Ecological Society of America, 1997, 78, 1946–1957.

[21] C. A. Klausmeier, *Regular and Irregular Patterns in Semiarid Vegetation*, Science, 2001, 284, 1826–1828.

[22] J. V. D. Koppel, J. C. Gascoigne, G. Theraulaz, M. Rietkerk, W. M. Mooij and P. M. J. Herman, *Experimental Evidence for Spatial Self-Organization and Its Emergent Effects in Mussel Bed Ecosystems*, Science, 2008, 322, 739–742.

[23] J. V. D. Koppel, M. Rietkerk, N. Dankers and P. M. J. Herman, *Scale-Dependent Feedback and Regular Spatial Patterns in Young Mussel Beds*, The American Naturalist, 2005, 165, E66–E77.

[24] V. Kostylev and J. Erlandsson, *A fractal approach for detecting spatial hierarchy and structure on mussel beds*, Marine Biology, 2001, 139, 497–506.

[25] B. V. Leeuwen, D. C. M. Augustijin, B. K. V. Wesenbeeck, S. J. M. H. Hulscher and M. B. D. Vries, *Modeling the influence of a young mussel bed on fine sediment dynamics on an intertidal flat in the Wadden Sea*, Ecological Engineering, 2010, 36, 145–153.

[26] L. Li and Z. Jin, *Pattern dynamics of a spatial predator-prey model with noise*, Nonlinear Dynamics, 2012, 67, 1737–1744.

[27] Q. Liu, E. J. Weerman, P. M. J. Herman, H. Oiff and J. V. D. Koppel, *Alternative mechanisms alter the emergent properties of self-organization in mussel beds*, Proceedings of the Royal Society B: Biological Sciences, 2012, 279, 2744–2753.

[28] Y. Lou and X. Zhao, *A reaction-diffusion malaria model with incubation period in the vector population*, Journal of Mathematical Biology, 2011, 62, 543–568.

[29] Z. Ma and R. Yuan, *Traveling wave solutions of a nonlocal dispersal SIRS model with spatio-temporal delay*, International Journal of Biomathematics, 2017, 10, Article ID 1750071.

[30] H. D. Paoli, T. V. D. Heide, A. V. D. Berg, B. R. Silliman, P. M. J. Herman and J. V. D. Koppel, *Behavioral self-organization underlies the resilience of a coastal ecosystem*, Proceedings of the National Academy of Sciences of the United States of America, 2017, 114, 8035–8040.

[31] Y. Peng, T. Zhang and M. O. Tade, *Existence of travelling fronts in a diffusive vector disease model with spatio-temporal delay*, Nonlinear Analysis: Real World Applications, 2010, 11, 2472–2478.

[32] R. M. Pringle, D. F. Doak, A. K. Brody, R. Jocque and T. M. Palmer, *Spatial Pattern Enhances Ecosystem Functioning in an African Savanna*, PLOS Biology, 2010, 8, e1000377.

[33] M. Rietkerk, M. C. Boerlijst, F. V. Langevelde, R. HilleRisLambers, J. V. D. Koppel, L. Kumar, H. H. T. Prins and A. M. D. Roos, *Self-Organization of Vegetation in Arid Ecosystems*, The American Naturalist, 2002, 160, 524–530.

[34] M. Rietkerk and J. V. D. Koppel, *Regular pattern formation in real ecosystems*, Trends in Ecology & Evolution, 2008, 23, 169–175.

[35] P. Rohani, T. J. Lewis, D. Grnbaum and G. D. Ruxton, *Spatial self-organisation in ecology: pretty patterns or robust reality?*, Trends in Ecology & Evolution, 1997, 12, 70–74.

[36] A. M. de Roos, E. McCauley and W. G. Wilson, *Pattern Formation and the Spatial Scale of Interaction between Predators and Their Prey*, Theoretical Population Biology, 1998, 53, 108–130.

[37] H. Shi and S. Ruan, *Spatial, temporal and spatiotemporal patterns of diffusive predatorCprey models with mutual interference*, IMA Journal of Applied Mathematics, 2015, 80, 1534–1568.

[38] M. L. Snover and J. A. Commito, *The fractal geometry of Mytilus edulis L. spatial distribution in a soft-bottom system*, Journal of Experimental Marine Biology and Ecology, 1998, 223, 53–64.

[39] G. Sun, Z. Jin, Q. Liu and L. Li, *Dynamical complexity of a spatial predator-prey model with migration*, Ecological Modelling, 2008, 219, 248–255.

[40] R. Wang, Q. Liu, G. Sun, Z. Jin and V. D. J. Koppel, *Nonlinear dynamic and pattern bifurcations in a model for spatial patterns in young mussel beds*, Journal of the Royal Society Interface, 2009, 6, 6705–718.

[41] Z. Wang, W. Li and S. Ruan, *Traveling Fronts in Monostable Equations with Nonlocal Delayed Effects*, Journal of Dynamics and Differential Equations, 2008, 20, 573–607.

[42] D. J. Wildish and D. D. Kristmanson, *Importance to Mussels of the Benthic Boundary Layer*, Canadian Journal of Fisheries and Aquatic Sciences, 1984, 41, 1618–1625.

[43] R. Wood and J. Widdows, *A model of sediment transport over an intertidal transect, comparing the influences of biological and physical factors*, Limnology and Oceanography, 2002, 47, 848–855.

[44] J. T. Wootton, *Local interactions predict large-scale pattern in empirically derived cellular automata*, Nature, 2001, 413, 841–844.

[45] J. P. Wright and C. G. Jones, *The Concept of Organisms as Ecosystem Engineers Ten Years On: Progress, Limitations, and Challenges*, Bioscience, 2006, 56, 203–209.

[46] G. Yang and J. Xu, *Analysis of spatiotemporal patterns in a single species reaction-diffusion model with spatiotemporal delay*, Nonlinear Analysis: Real World Applications, 2015, 22, 54–65.

[47] J. Zhang, W. Li and X. Yan, *Multiple bifurcations in a delayed predator-prey diffusion system with a functional response*, Nonlinear Analysis: Real World Applications, 2010, 11, 2708–2725.

[48] C. Zhu, L. Li and F. Yang, *Traveling waves in a nonlocal dispersal SIRH model with relapse*, Computers & Mathematics with Applications, 2017, 73, 1707–1723.